Aus der V. Medizinischen Klinik

der Medizinischen Fakultät Mannheim

(Direktor: Prof. Dr. med. Bernhard Krämer)

The use of Mesenchymal Stromal Cells to ameliorate Diabetic Kidney Disease in the BTBR$^{ob/ob}$ model

Inauguraldissertation

zur Erlangung des akademischen Grades

Doctor scientiarum humanarum (Dr. sc. hum.)

der

Medizinischen Fakultät Mannheim

der Ruprecht-Karls-Universität

zu

Heidelberg

vorgelegt von

Diego O. Pastene Maldonado

aus

Santiago de Chile

2021

Dekan: Prof. Dr. med. Sergij Goerdt

Referenten: Prof. Dr. med. Bernhard Krämer

Table of Contents

Abbreviations

BW	body weight
BTBR	black and tan brachyuric
DKD	diabetic kidney disease
ESRD	end-stage renal disease
ECM	extracellular matrix
FITC	fluorescein isothiocyanate
GBM	glomerular basement membrane
GFR	glomerular filtration rate
hABCB5$^+$	human dermis-derived stromal cell
hADSC	human adipose-derived stromal cell
HbA1c	glycated hemoglobin
LSM	least square means
MSC	mesenchymal stromal cells
OB	obese phenotype of BTBR
PAS	periodic acid-Schiff
STZ	streptozotocin
U-ACR	urinary albumin-creatinine ratio
WT	wild-type phenotype of BTBR

1. Introduction

1. Diabetes and diabetic complications

Diabetes mellitus is a pathological condition of diverse etiology [1], and is characterized by the impairment to control blood glucose levels due to the absence or ineffectiveness of insulin. More than four hundred millions of people live with diabetes today. According to projections, this number will increase to ca. 700 million by 2045 [2]. Diabetes is diagnosed when sustained hyperglycemia is present i.e. blood glucose ≥126mg/dL after 8h fasting and/or glycated hemoglobin (HbA1c) ≥6,5% [3]. The main forms of diabetes that prevail are type-2 diabetes, type-1 diabetes and gestational diabetes. Unlike the first two types, gestational diabetes is usually transient, and soon after child delivery, blood sugar levels return to normal. Type-1 diabetes is mostly due to an autoimmune response that causes destruction of pancreatic ß-cells. In contrast, in type-2 diabetes insulin is still produced but less effective in controlling blood glucose levels, a phenomenon known as insulin resistance. Although initially patients with type-2 diabetes may not need insulin therapy, at later stages insulin treatment is usually installed because of progressive ß-cell dysfunction.

Irrespective of the form, severe hyperglycemia is a continuous life-threatening condition, which needs to be monitored and treated for its acute complications e.g. diabetic ketoacidosis and hyperosmolar hyperglycemic state [4]. Tight glycemic control on diagnosed diabetic patients considerably seclude the frequency and intensity of acute events. However, long-standing hyperglycemic blood glucose levels may initiate silent vascular lesions that may escalate into severe complications. From the different tissues in organisms, the vascular system is arguably the most affected by chronic hyperglycemia. Long-standing diabetes dramatically increases the risk of developing atherosclerosis, cardiovascular disease, and is the major cause of complications comprising the microvasculature in kidneys (nephropathy), retina (retinopathy), and peripheral nerves (neuropathy). Such complications are a set of well-reported major afflictions, which progress because of lesions in small vessels, and the action of high glucose at cellular level [5].

2. Diabetic kidney disease

Diabetic kidney disease (DKD, formerly known as diabetic nephropathy) is the single foremost cause of end-stage renal disease (ESRD) in the United States [6]. The progression from the early stages of DKD to ESRD follows characteristic histopathological changes in the kidney [7], which correlates with most of the detectable clinical parameters studied [8]. The mechanisms leading to nephropathy in diabetes and its progression have been extensively studied over the years, and share common processes described for most of the microvascular associated complications of diabetes mentioned before (notably at cellular and molecular level) [9] . The hyperglycemic environment exerts a plethora of alterations that extends ubiquitously to all tissues unable to cope with glucose, or its intermediate metabolites [10]. In the kidney, the endothelium and the mesangium have initially been flagged as the two most affected cell-types due to their inability to regulate glucose uptake [11, 12]. This was shown by *in vitro* studies where mesangial cells overexpressing GLUT1 in a non-hyperglycemic environment had increased extracellular matrix production by overutilization of glucose [13]. Later studies further expanded the consequences of hyperglycemia to podocyte injury [14].

3. Histopathology and pathophysiology of DKD

3.1.   Characteristic histopathology

Histopathology shows that the earliest detectable changes occur in the glomerulus, i.e. thickening of the glomerular basement membrane (GBM) followed closely by mesangial matrix expansion. Podocyte lesions are also characteristic in DKD although visible changes only appear at later stages.

The GBM is the non-cellular structure situated between the fenestrated endothelium, and the foot process of podocytes surrounding the capillary tuft [15]. In addition, the GBM is one of the components of the glomerular filtration barrier: a mechanical and anionic sieve which ultrafiltrates small size molecules and water from plasma. Alterations in extracellular matrix (ECM) production by podocytes and the fenestrated endothelium contributes to an irregular thickening of the GBM that is noticeable 1-2 years after the onset of diabetes [7] . It has been suggested that thickening of the glomerular basement might correspond to an adaptation to shear stress forces and

podocytes injury to reduce podocyte detachment [16]. Yet, the role of glucose in the production or modification of ECM proteins, and therefore thickening of the GBM, cannot be excluded.

Another clearly modified structure in DKD is the expansion of the mesangial portion of the glomerulus. Similar to GBM thickening, mesangial expansion may occur as consequence of increased or altered ECM deposition by mesangial cells, or direct glycation of ECM components [17]. In early lesions, mesangial matrix expansion is mostly diffuse and may become nodular at later stages (also referred as Kimmelstiel-Wilson nodules) partially occluding the capillaries in the glomerular tuft. Although within one kidney mesangial matrix expansion is heterogeneous amongst the different glomeruli, with progression of DKD the number of glomeruli with nodular lesions will increase [7]. In line with the Brenner hyperfiltration hypothesis [18], which states that the loss of glomerular filtration units might induce glomerular hypertrophy as a compensatory mechanism, glomerular size is increased in patients with DKD as well as in most of DKD models.

Glomerular basement thickening and expansion of the mesangium lead to gradual scarring of the glomerulus culminating in glomerulosclerosis, and loss of glomerular function. Loss of the interdigitating organization of podocyte foot processes, i.e. foot process effacement, is directly linked to the loss of permselectivity of the GBM and occurs in all renal diseases that are accompanied by proteinuria [19]. It is however not clear if podocyte effacement is a mechanical adaptation to increased intraglomerular pressure, or podocyte injury [14, 20]. Irrespective of the cause, foot process effacement reduces podocytes anchoring to the GBM, which will foster their detachment [20].

3.2.   Characteristic pathophysiology

The extension of the structural changes described above will have a clear impact in several physiological parameters evaluated in DKD. One of the most classical parameters to evaluate DKD is proteinuria, which is indicative of protein leakage from the plasma. In a healthy kidney, only a small fraction of plasma proteins reaches the tubular portion where it is reabsorbed by the proximal tubule's epithelial cells [21]. In diseased kidneys, the glomerular filtration barrier is impaired allowing the free filtration of plasma proteins. Because the amount of filtered proteins surpasses the reabsorbing capacity in the proximal tubules, proteins are excreted in urine. Loss of

permselectivity of the glomerular filtration barrier is caused by reduced charge of endothelial glycocalix, foot process effacement (and podocyte detachment), and glycation of heparan sulfate proteoglycans in the GBM, or a combination of them [22-24]. In patients with overt proteinuria, ultrafiltrated protein may also impose damage to the tubular compartment in many ways, ranging from initiation of inflammation to complement activation in tubular cells [25, 26].

A second key pathophysiological process that may aggravate progression of kidney disease in diabetes is hyperfiltration. In healthy individuals, the afferent and efferent arterioles slightly differ in blood flow resistances, being lower in afferent arterioles. This helps to maintain a stable intraglomerular pressure required for filtration. This difference in resistance is tightly regulated by systemic control (importantly the sympathetic nervous system and the renin angiotensin aldosterone system) and local mechanisms involving sodium concentration in the plasma filtrate (i.e. via the tubuloglomerular feedback) [27]. Hyperfiltration in diabetes occurs in the presence of systemic comorbidities such as hypertension and obesity through the release of vasoactive factors (i.e. angiotensin II). These factors particularly mediate constriction of the efferent arteriole, ultimately raising intraglomerular pressure. The situation aggravates in diabetes as a consequence of glucose and sodium reabsorption via the sodium-glucose cotransporter 2 [28]. Increased sodium reabsorption in proximal tubules results in diminished sodium delivery at the macula densa in the distal convoluted tubule, which subsequently signals to dilate the afferent arteriole in order to increase glomerular blood flow. Moreover, high levels of glucose also upregulate the expression of the sodium-glucose cotransporters as a compensatory mechanism to reduce glucose excretion. This further leads to reduced sodium reabsorption in the distal convoluted tubule, thus promoting vasodilation and disrupting the so-called tubuloglomerular feedback of glomerular blood flow [29].

The proposed mechanism of hyperfiltration implies that increased intra-glomerular pressure might precede most of the classic histopathologic characteristics of the disease, including thickening of the GBM. Moreover, hyperfiltration may occur while hyperglycemic levels are below threshold levels of diabetes (prediabetes) [30, 31].

4. Clinical parameters of DKD

The progression of DKD is usually monitored by renal function, i.e. glomerular filtration rate (GFR), and by the extent of filtration barrier impairment i.e. albuminuria. GFR is the measure of kidney function for effective free fluid-filtration. It fundamentally depends on the filtration surface (functional number of glomeruli), and blood flow. In humans, the average GFR is 125 mL/min/1,73m^2 for men younger than 40 years of age. Gender and age also determine the normal GFR, which decreases after 40 years of age. Hyperfiltration and hypertension affects GFR in diabetic kidneys by increasing blood flow. "Whole kidney" hyperfiltration starts without loss of functional glomeruli, is subject to daily fluctuations, and is difficult to assess because of inaccuracy of serum creatinine-based GFR estimates [32]. As glomerular damage commences, hyperfiltration increases at the single nephron level to compensate for the loss of functional nephrons. This will continue until the number of functional glomeruli is too low to maintain renal filtration constant, resulting in a decline in kidney function.

The presence of albumin in urine is also a good parameter to study the progression of DKD. Based on the glomerular sieving coefficient for albumin, it is estimated that only ~3% of plasma albumin passes through the glomerular filtration barrier. In healthy humans, urinary albumin excretion does not exceed 30 mg/day (normoalbuminuria). Many studies have highlighted albuminuria as a predictor of chronic kidney disease outcome and progression, particularly for DKD [21]. High concentrations of albumin in tubules contributes to scarring and inflammation due to its nephrotoxic properties, but also indicates the ultrafiltration of many other biologically active molecules (e.g. complement factors) that may contribute to nephropathy [22]. Although threshold values have been defined to characterize the stages of DKD, normoalbuminuric patients with developing DKD have also been reported [33].

Animal models have been very helpful in delineating the complexity of DKD, as they can be used to evaluate susceptibility loci by gene targeting and for the evaluation of new therapeutic options to ameliorate or prevent disease progression.

5. Methodologies used to study DKD

5.1.   Animal models for DKD

Several models of DKD in rodents have been described, each with its advantages and flaws. Mice models are preferentially employed for mid to short-term studies due to their rapid breeding rate and DKD progression. The most widely used among them is the Streptozotocin (STZ)-induced type-1 diabetic model that can be generated by the peritoneal injection of STZ. It is a versatile model because it can be produced in several mouse strains with different degrees of susceptibility to DKD [34]. Other genetically induced type-1 models such as de Akita and OVE23 FVB mice are much more effective to develop histopathologic features than STZ mice. Regarding type-2 diabetes, most of the models are generated through induction of obesity by different mechanisms (e.g. high fat diet, leptin feedback deficiency, dysfunctional insulin receptors) [35]. An interesting characteristic of these models is that they can be used to profile the genetic expression of disease, and by comparison with other models, evaluate allelic variants protecting from or sensitizing for the progression of DKD. Aggravation with knock-out or knock-in strategies is also a valuable resource in these models. For example, the endothelial nitric oxide synthase (eNOS) knock-out, which highlights the contribution of endothelial dysfunction to the progression of the disease [36], or the human serum carnosinase (CN1) transgenic [37] have been used.

5.2.   GFR assessment

Determination of GFR in mice is a cumbersome task mainly derived from the constant and excessive animal handling (introducing stress as a variable), and further analysis of samples. Clearance of exogenous compounds are preferably used for the determination of GFR in mice, as endogenous markers such as creatinine tend to overestimate glomerular filtration because of tubular secretion [38]. Inulin-like compounds or non-isotopic iodinated tracers are among the effective substances to determine this parameter, which consist in timed-repeated blood sampling and determination by chromatography or similar methods [39, 40]. An improvement to this necessity is coupling these compounds with a fluorescent moiety such as fluorescein isothiocyanate (FITC), which enhances detection, reduces blood sampling and the need for expensive equipment [41]. A different approach published by Schreiber et al. [42] employs a transcutaneous device to record the clearance rate of a FITC-

linked compound to estimate GFR, thus minimizing animal handling and reducing stress-derived bias.

5.3.   Histology and microscopy for DKD lesions

The most widely accepted procedure for histopathological assessment is classic histology. Classic histology can be described as the routinely methodologies that comprehend thin sectioning of a tissue, chemical staining and bright-field microscopy imaging to study the microstructure of biological tissues. From the many options, Periodic acid-Schiff (PAS) staining is one the most popular to evaluate ECM alterations in kidneys. Although the original protocol was established more than 70 years ago [43], the principles remain unchanged up to this day to evaluate kidney pathological lesions. PAS protocols (and the whole compendia of classic histological techniques) have received much improvement from their origins by automatization, speed enhancements, and digitalization thus making them the easiest method of choice. Still, several limitations exist. First, histopathological changes require skilled personnel for assessment scores to determine the extension and grade of glomerular lesions, which restrict the analysis to qualitative differentiation. Nevertheless, it is worth mentioning that great improvements in digital analysis using artificial intelligence (deep learning approaches) have been achieved to supplement pathologic scores with quantitative information [44]. A second inconvenience is that thin slicing requires trained personnel since it cannot be fully automatized to prevent artifacts and excessive time investment. A third restriction (and perhaps the most important) is the two-dimensional level of information, which decreases robustness of the analysis when certain morphometric parameters are studied (i.e. tuft size and exact vessel diameter). A complementary approach to some of these issues is three-dimensional histology by a combination of dark-field microscopy, fluorescent staining and optical tissue clearing [45]. Fluorescent staining and dark-field microscopy are two already consolidated fields in histology employed in the analysis of thin sections. Their uses range from: antibody staining of one or more proteins of interest, to contrast enhancement with generic dyes such as DRAQ5-Eosin [46] or the autofluorescence of tissues like kidneys [47]. In contrast, optical tissue clearing, a method that seeks to reduce the natural light scattering properties of tissues [45], is a novel discipline in tissue histology. This allows scanning of tissues in a three-

dimensional fashion using dark-field confocal or light sheet microscopes, without the necessity of thin slicing.

These methodologies described above are complementary approaches to evaluate the progression of DKD.

6. Treatment of DKD

6.1. Conventional therapeutic options

Although hyperglycemia is in principle the cause of DKD, treatment with classic glucose-lowering drugs (such as metformin, sulfonylureas, thiazolidinediones and others) may lead to hypoglycemia and may have the disadvantage of increasing the risk for cardiovascular events [48]. This contrasts with the evidence of several clinical trials confirming that glucose-lowering strategies in diabetes patients ameliorates microvascular complications [49]. Newer antihyperglycemic drugs mimicking the effect of glucagon-like peptide-1 have a considerable efficacy in lowering blood glucose, and reducing albuminuria in early stages of DKD [48]. Finally, sodium glucose cotransporter-2 inhibitors are very effective drugs in DKD due to their double effect on blocking glucose reabsorption and reducing single nephron hyperfiltration by restoring tubuloglomerular feedback [50]. Despite of being recommended as an ideal second-line treatment, they are not exempt of side effects like increase of genital infections and risk of diabetic ketoacidosis in euvolemic diabetes patients [51]. Blood pressure is directly linked to glomerular hyperfiltration. Among the different anti-hypertensive drugs available, renin-angiotensin-aldosterone system inhibitors, which ultimately reduce the effect of angiotensin II, are widely-used due to their proven efficacy [52]. In chronic kidney disease, postglomerular vascular resistance increases hyperfiltration by the effect of several mediators, in particular angiotensin II [29]. Treatment of DKD includes the use of angiotensin converting enzyme inhibitors, angiotensin II type-1 receptor blockers, and renin inhibitors. Although effective in their use to reduce albuminuria and to slow down the progression to ESRD, they increase the risk of acute kidney injury due to hypoperfusion, and hyperkalemia [52]. The benefit of other blood pressure lowering drugs (e.g. diuretics) on renal end-points is less well-known. Likewise, there is no general consensus whether the use of ß-blockers apart from lowering blood pressure have additional benefits on the progression of DKD [53].

6.2.   Regenerative approaches for DKD

Resolution of established renal lesions in patients with diabetes has initially been reported for type-1 diabetic patients after pancreatic transplantation, or a to a lesser extent after treatment with angiotensin converting enzyme inhibitors and further confirmed in animal models [54]. Further studies in rodent models also confirmed regression of glomerulosclerotic lesions and capillary regeneration with the same treatment [55]. These findings have led to the discovery of renal progenitor cells within the developed kidney, recruited to specialize into glomerular cell lineages such as podocytes [56, 57]. Nonetheless, the concise mechanisms to induce remission of established renal lesions are still lacking.

6.3.   The use of multipotent mesenchymal cells for DKD

Adult multipotent mesenchymal cells (also known as mesenchymal stromal cells, MSC) are a tempting approach to induce tissue regeneration, because of their proven in-vitro differentiation potential, paracrine secretion of bioactive molecules, and immunomodulatory mechanisms [58]. MSC from distant tissues such as bone marrow are also capable to migrate to the kidneys, thus contributing to repair of kidney injuries *in situ* [59]. These properties make them suitable candidates to elicit the self-regeneration of kidneys, or as an exogenous therapy in chronic kidney damage.

The use of mesenchymal stromal cells to ameliorate DKD is not new. Since the first published experiment, different approaches using MSC have been tested, using different cell dosage, cell types, model strains, xenogeneic treatments, and many other variables (Table 1). Interestingly, 22 out of 23 research papers from more than 10 independent research groups have found positive outcomes from the use of mesenchymal stromal cell-based therapies, with the notable exception of observed tubular necrosis in a subset of treated animals [60]. The level of amelioration in DKD ranges from improvement at physiological levels (blood glucose normalization and reduced proteinuria) to reduced histological features of DKD. From the latter, at least 80% of the reviewed studies reported reduction in ECM deposition associated to pathological features (e.g. mesangial matrix expansion). Noteworthy among the possible underlying mechanisms are: differentiation into ß-cell with insulin production

[61], cell homing after tail vein injection [62], podocyte stabilization [63], and release of paracrine factors [64].

An interesting observation of the landscape of published studies is that most of the studies have been performed in STZ-induced diabetes, while the use of MSC in spontaneous diabetic models has been relatively neglected. This direction in research leaves gaps that need to be filled by incorporating spontaneous models, insulin resistant models, and alternative mesenchymal stromal cell sources to confirm their use as a viable therapy.

Table 1 – Summary of systematically reviewed literature of mesenchymal stromal cell interventions on DKD models

Year	Ref.	Animal model	Cell type	Treatment	End-point improvement
2006	[61]	Mouse T2D (aggravated with STZ)	hBMDSC (Xenogeneic)	2.5×10^6 cells (2 times)	Lowered hyperglycemia, increased insulin production. Decreased pathological lesions in pancreas and glomeruli (reduction of mesangial expansion).
2008	[65]	Mouse T1D (STZ)	BMDSC (syngeneic)	0.5×10^6 cells	Reduced urinary albumin-creatinine ratio (U-ACR), normalization of blood glucose and glucosuria, decreased hyalinosis and mesangial expansion. Partial pancreatic tissue regeneration.
2009	[60]	Mouse T2D (db/db)	BMDSC (syngeneic)	1×10^6 cells	Improved insulin sensitivity. Reduced U-ACR.
2009	[66]	Mouse T1D (STZ)	BMDSC (syngeneic)	0.5×10^6 cells	Significant decrease of U-ACR. Reduced glomerulosclerosis and mesangial expansion.
2009	[67]	Rat T1D (STZ)	BMDSC (syngeneic)	2×10^6 cells	Transient reduction of U-ACR and transient normalization of glucose. Apparent mesangial expansion and glomerulosclerosis reduction.
2010	[68]	Mouse T1D (STZ)	Bone marrow (syngeneic)	10×10^6 cells	Reduced blood glucose levels and apparent reduction of kidney hypertrophy.
2012	[69]	Rat T1D (STZ)	ADSC (autologous)	10×10^6 cells	Reduction of blood glucose and increase of insulin production. Apparent decrease in glomerular enlargement.
2012	[70]	Rat T1D (STZ)	hUCB-MNC (Xenogeneic)	150×10^6 cells	Reduced U-ACR, normalization of blood glucose. Decreased mesangial expansion and glomerulosclerosis.

Year	Ref.	Animal model	Cell type	Treatment	End-point improvement
2012	[62]	Rat T1D (STZ)	hUCB-MNC (Xenogeneic)	$0.5x10^6$ cells	Apparent 24 hrs. proteinuria reduction. Reduced mesangial expansion and glomerulosclerosis.
2013	[71]	Rat T1D (STZ)	BM-MSC (syngeneic)	$2x10^6$ cells (double injection)	Reduced blood glucose. Reduced 24hr. albuminuria and improvement of creatinine clearance. Reduced mesangial expansion.
2013	[72]	Rat T1D (STZ)	BM-MSC (syngeneic)	$2x10^6$ cells	Reduced U-ACR and improvement of creatinine clearance. Reduced mesangial expansion, glomerulosclerosis, GBM thickening, foot process effacement and increased podocyte density in treated kidney.
2013	[73]	Rat T1D (STZ)	hADMSC (Xenogeneic)	$0.5x10^6$ cells (5 times every four weeks)	Reduced 24hr. albuminuria and improvement of creatinine clearance. Reduced glomerular enlargement.
2013	[74]	Rat T1D (STZ)	BM-MSC (syngeneic)	$1x10^6$ cells	Reduced U-ACR. Apparent reduction in mesangial expansion and glomerulosclerosis.
2014	[75]	Rat T1D (STZ)	BM-MSC (syngeneic)	$1x10^6$ cells	Reduced 24hr. albuminuria and improvement of blood glucose. Apparent reduction of mesangial expansion.
2014	[76]	Rat T1D (STZ)	BM-MSC (syngeneic)	$2x10^6$ cells (double injection)	Reduced 24hr. albuminuria, improvement of blood glucose and creatinine clearance. Reduction of glomerulosclerosis.
2014	[77]	Rat T1D (STZ)	BM-MSC (syngeneic)	$2x10^6$ cells (double injection)	Reduced 24hr. albuminuria, improvement of blood glucose and creatinine clearance. Reduction of glomerulosclerosis.
2014	[78]	Shrew T1D (STZ)	BM-MSC (syngeneic)	$5x10^6$ cells (double injection)	Reduced 24hr. proteinuria, improvement of blood glucose and insulin production. Reduction of glomerular enlargement.
2015	[63]	Mouse T1D (STZ)	BM-MSC (syngeneic)	$0.5x10^6$ cells	Reduced U-ACR. Reduction of mesangial expansion and increased number of podocytes per glomerular volume.
2015	[79]	Rat T1D (STZ)	ADMSC (autologous)	$10x10^6$ cells	Unspecific reduction of glomerular lesions.
2016	[80]	Rat T1D (STZ)	BM-MSC (syngeneic)	$1x10^6$ cells	Blood glucose improvement and insulin production. Reduced 24hr. albuminuria.

Year	Ref.	Animal model	Cell type	Treatment	End-point improvement
2016	[81]	Rat T1D (STZ)	Exosomes of hUrine-SC (Xenogeneic)	100 µg exosomes weekly	Reduced U-ACR. Reduction of mesangial expansion. Decreased TUNEL positive histology.
2016	[82]	Rat T1D (STZ)	BM-MSC (Autologous)	$2x10^6$ cells	Unspecific reduction of glomerular lesions. Reduced 24hr. proteinuria.
2016	[64]	Mouse T1D (STZ)	BM-MSC (Xenogeneic)	$0.01x10^6$ cells/g BW (2 times) and conditioned media	Reduced U-ACR.
		Mouse T2D (HFD)	BM-MSC (Xenogeneic)	$0.01x10^6$ cells/g BW (4 times) and conditioned media	Reduced U-ACR. Blood glucose improvement. Reduction of mesangial expansion and glomerulosclerosis.
2017	[83]	Mouse T1D (STZ)	Diabetic / normal / supplemented WJ - BMDSC (Xenogeneic) from NIDDM model	$0.01x10^6$ cells/g BW (4 times)	Reduced U-ACR.
		Rat T1D (STZ)	Diabetic / normal / supplemented WJ - BMDSC (allogeneic) from NIDDM model	$0.01x10^6$ cells/g BW (4 times)	Reduced U-ACR.
		Rat T2D (OLETF)	Diabetic / normal / supplemented WJ - BMDSC (Allogeneic) from NIDDM model	$0.01x0^6$ cells/g BW (4 times)	Reduced U-ACR.

7. Aim of the study

As it has been reviewed from the literature (Table 1), the use of MSC for the amelioration of DKD seems to be a viable therapeutic option, showing improvement of pathologic features at histological and physiological levels. However, the experimental settings overly recur to a combination of non-spontaneous type-1 diabetic models and bone marrow-derived MSC. Strikingly, at least 90% of all diabetes cases are in fact type-2 diabetes, emphasizing the need to study the therapeutic efficacy of mesenchymal stromal cells as treatment option for patients with this type.

In this work, we have hypothesized that an intervention with human MSC on mid stages of DKD in a type-2 diabetic model will decrease the progression of the disease as it has been shown in type-1 diabetic models. To address this hypothesis, we conducted two independent experiments in obese black and tan brachyuric (BTBR) mice, to evaluate the efficacy of two different human MSC: adipose-derived

(hADSC) and dermis-derived (hABCB5+). In view of the limitations to estimate GFR in rodent models and to improve histologic analysis of lesions in a robust three-dimensional fashion, this project incorporates some of the newest methodologies available to assess GFR and to display renal tissue in a three-dimensional manner. The methods implemented are:

- Transcutaneous determination of the clearance of an exogenous tracer.
- Solvent-based tissue clearing of whole tissues, pre-stained with a fluorescent dye, and imaged by confocal and light-sheet dark-field microscopes.

The efficacy of MSC interventions, and the success of the implemented procedures, will be addressed by answering the following questions:

1) Is an intervention with MSC able to ameliorate conventional renal endpoints of DKD in the BTBR$^{ob/ob}$ model?
   a. Are MSC reducing albuminuria excretion or hyperglycemia?
   b. Does GFR measurement show signs of slowed progression of renal damage in this model?
   c. Can we observe a reduction in glomerular histopathological changes by treatment?

2) Do different MSC have the same outcome?
   a. Can hADSC reduce hyperglycemia, albuminuria and glomerular lesions observed in the BTBR type-2 diabetic mice model?
   b. Are hABCB5+ MSC able to improve hyperglycemia, albuminuria and glomerular lesions observed in the BTBR type-2 diabetic mice model?

2. Material and methods

1. Equipment

Equipment	Manufacturer
A1cNow+ monitoring kit	PTS-diagnostics, United States
Anesthetic isoflurane vaporizer	CP-pharma, Germany
Clover HbA1c analyzer	Infopia, South Korea
Confocal microscope – TCS SP8	Leica microsystems, Germany
Eppendorf centrifuge 5415R	Eppendorf, Germany
Heating chamber Heraeus	Kendro laboratory products, Germany
Heating plate	MEDAX GmbH, Germany
Jun-Air compressor	Rio grande, United States
Light sheet microscope – DLS TCS SP8	Leica microsystems, Germany
OneTouch Verio IQ meter	LifeScan Europe, Italy
Richert-Jung Biocut 2030	Leica microsystems, Germany
Slide scanner Aperio VERSA	Leica microsystems, Germany
Syringe pump Fusion 100	Chemyx, United States
Tecan Infinite M200	Tecan, Switzerland
Tissue processor TP1020	Leica microsystems, Germany
Transdermal GFR monitor	Medibeacon GmbH, Germany

2. Animal model description

The BTBR strain is a natural hyperinsulinemic mouse compared to the classic C57BL/6 mouse. The selection of the homozygotic "ob" mutation induces leptin deficiency, which leads to morbid obesity and sustained hyperglycemia. Renal histopathology of the BTBRob/ob closely resembles the pathological lesions described in human DKD such as mesangial expansion, glomerular hypertrophy and podocyte loss among others. Functional parameters, like persistent albuminuria, are also present in the BTBRob/ob since 8 weeks of age [84].

3. Mesenchymal stromal cells

Human adipose-derived MSC

Professor Karen Bieback from the Institute of Transfusion Medicine and Immunology, (Medical Faculty Mannheim, Heidelberg University) kindly provided human adipose-derived MSC for this project. The complete description of isolation is described elsewhere [85-87]. Briefly, cells were isolated from human lipoaspirates obtained from healthy donors who underwent liposuction surgery. The raw lipoaspirate was thoroughly washed with phosphate buffer-saline and then treated with an equal part of collagenase type I solution for 45-60 min at 37°C, (1:1 volume, 0.15% collagenase). Inactivation of the collagenase was achieved by addition of an equal part of DMEM/10% AB human serum. Sequential steps of centrifugation, pellet reconstitution, and sieving (100µm cell strainer) were used to refine the cell content (also known as stromal vascular fraction). The stromal vascular fraction was then resuspended in 10% AB human serum/stem cell medium and plated in a T25 or T75 culture flasks. Extensive washings steps were performed the day after seeding to discard non-adherent cells. Cells were characterized by fluorescence-activated cell sorting for stem cells markers and assays were performed for adipogenic, chondrogenic and osteogenic differentiation. Finally, five donors-pool was expanded in FBS-free medium for 14 days and resuspended in phosphate buffer-saline shortly before injection.

Human dermis-derived mesenchymal stromal ABCB5+ cells

The company Ticeba-REHACELL GmbH&Co (Heidelberg, Germany) kindly provided hABCB5+ cells for this project. The isolation procedure has been described elsewhere [88]. Briefly, hABCB5+ cells were obtained from healthy patients undergoing medical intervention resulting in leftover skin tissue. Afterwards, skin tissue was separated from subcutaneous adipose tissue, disinfected, washed, dissected and enzymatically digested. Then, cells were centrifuged and expanded in stem cell-selecting growth media. hABCB5+ cells were isolated by antibody-coupled magnetic bead sorting, using a mouse-anti-human ABCB5 monoclonal antibody. Purity of the isolated cells was determined by flow cytometry, setting a 90% as optimal. After purity assessment, cells were cryopreserved in liquid nitrogen. Cells

were thawed, washed and resuspended in Ringer's lactate solution shortly before injection.

4. Animal experiments

All experiments and methods conducted were performed in accordance with guidelines and regulations, and formally approved by the "Regierungspräsidium Karlsruhe" (AZ 35-9185.81/**A-3/15**, AZ 35-9185.81/**G-108/13** & AZ 35-9185.81/**G-199/19**). Mice used for tissue clearing implementation, handling and methodological training were selected from project **A-3/15**.

4.1.   Interventional study

Two cohorts of 8-week-old male (n=20) BTBR$^{ob/ob}$ mice (BTBR.Cg-*Lep^{ob}*/WiscJ, stock number: 004824) were purchased from The Jackson Laboratory (Bar Harbor, ME, USA) between 2017-2018 (**G-108/13**) and 2019-2020 (**G-199/19**). Figure 1 summarizes the experimental design for cohorts treated with human adipose-derived MSC (cohort hADSC) or human dermis-derived stromal cells (cohort hABCB5+). Animals were housed for 3 weeks before experimentation for acclimatization purposes in a 12-hour light cycle environment, and given food and water *Ad libitum*. Mice were randomly allocated to a group who would receive a dosage of mesenchymal stromal cell suspension or control (hereupon "OB treated" or "OB control", respectively) before the start of the experiment (n=10).

MSC intervention was performed at 12 weeks of age in both experimental settings. Mice from "OB treated" group in the hADSC cohort received 0.5×10^6 hADSC cells suspended in 0.2mL phosphate buffer-saline via tail vein. Analogously, "OB treated" mice in hABCB5+ cohort received 1×10^6 hABCB5$^+$ cells in 0.2mL Ringer's lactate solution. OB control groups received same volume of vehicle solution (phosphate buffer-saline or Ringer's lactate solution).
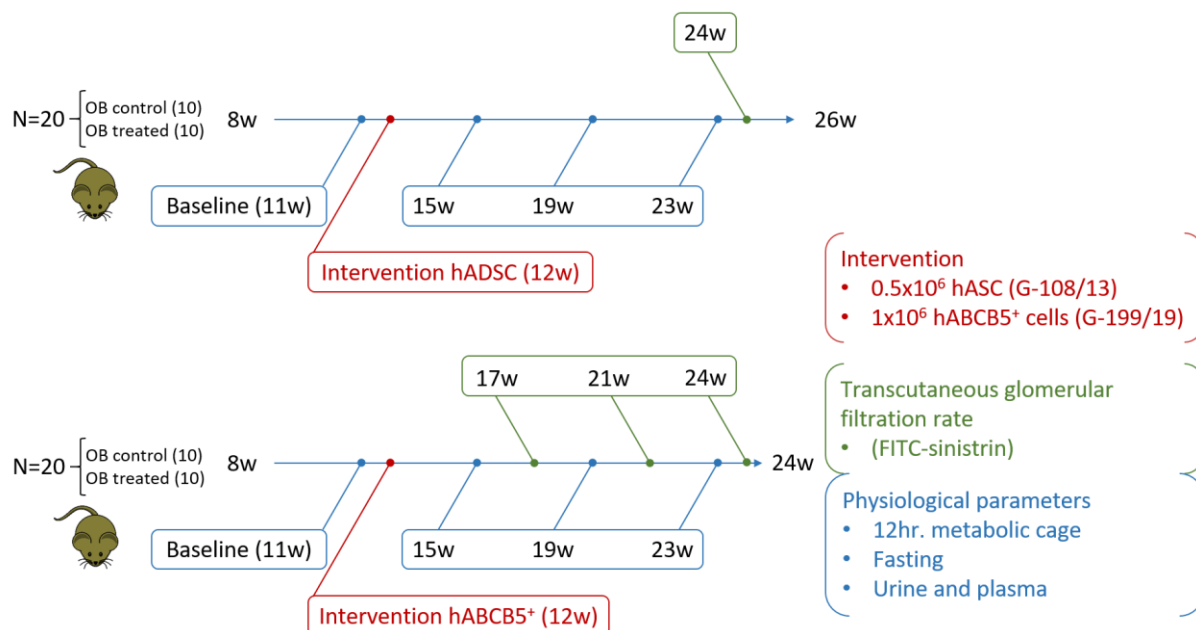
Figure 1 – Interventional studies on the BTBR^ob/ob. Physiological parameters (blue) were collected every 4 weeks after fasting. HbA1c was evaluated at baseline and after 12 weeks. Intervention (red) was performed at 12 weeks of age in both cohorts. GFR (green) was evaluated at 24 weeks (cohort hADSC) or 17, 21 and 24 weeks (cohort hABCB5+). Histology was examined at the end of the experiment (either 26 or 24 weeks).

Urine and blood were collected every four weeks from 11 to 23-weeks of age after 12 hours fasting in a metabolic cage during the dark phase. Transcutaneous GFR was compared at 24-weeks of age in cohort hADSC or measured sequentially at 17 weeks and 21 weeks in cohort hABCB5+ between diabetic groups. Additionally, the GFR of a wild-type group was evaluated at 21-weeks age (n=3) to be compared with values in cohort hABCB5+.

Two composite end-points were chosen under the welfare legislation for experiment termination after mice have been allocated: i) 12-14 weeks after treatment induction or ii) high scoring in weekly-checked health criteria (Table 2). Following this guideline, mice reaching the first end-point were perfused at 24-26 weeks of age and kidneys (among other tissues) were collected for histology.

Table 2 – Animal Health criteria assessment

Criteria*	Description
Nutrition	Weekly weight of the mice.
Condition	General physical aspect (e.g. fur) and examination (e.g. bulks).
Environment	Interaction with elements present in the environment.
Sociability	Interaction with other mice present in the environment.
Movement	Flee response and general movement.
Breathing	Thoracic movement while resting.
Feces	Consistency of fecal waste.
Wounds	Presence of wounds and degree.

*Each parameter is scored weekly from 0-3 being 0 the healthiest and 3 the worst condition.

4.2.   Transcutaneous GFR estimation

Schreiber et al., (2012) [42], described the method employed in this project to measure the GFR in mice. The methodology makes use of an inulin-like compound (sinistrin), covalently bound to a fluorophore (FITC-sinistrin, Fresenius Kabi, Austria) that enables its transcutaneous tracking through a miniaturized sensor placed over the naked skin of the mice. As inulin, sinistrin is not reabsorbed (nor excreted) and freely filtered from plasma. Two blue-light emitting diodes incorporated on the device emit sequential pulses of a specific wavelength range that excites the fluorescent moiety of the compound, while a central photosensitive diode records the emitted fluorescence that is later stored in an internal memory.

Figure 2 displays the clearance profile of the molecule in conscious mice. A peak after administration via tail vein indicates a successful delivery into the blood stream of the animal, which is followed by an excretion phase in which the signal decays back to baseline. The whole process can be modelled using a three-compartment equation, where the half-life time of the linear decay phase is used for the determination of the GFR. The half-life time in minutes together with a semi-empirical conversion factor for mice and the weight of the animal allow to estimate the GFR (Eq.1 adapted from [42]). A complete description of the protocol can be found in reference [89].
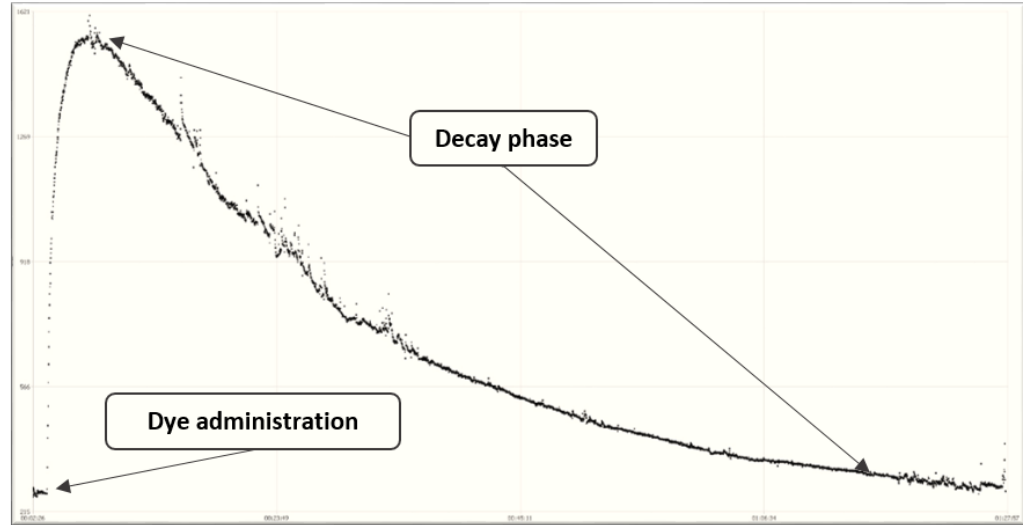
Figure 2 – Transcutaneous tracking of FITC-sinistrin fluorescence. The half-life time of the linear decay phase estimates the clearance rate of the dye in the animal after administration.

$$\text{GFR}[\mu\text{L} \cdot \text{min}] = \frac{14616.8\left[\frac{\mu\text{L}}{100\text{g bw}}\right]*\text{mice body weight [g]}}{\text{t}_{1/2}(\text{FITC--sin})[\text{min}]} \quad (\text{Eq.1})$$

4.3.   Collection of samples and tissues

Blood sampling was performed by puncture of the *vena facialis*, and ca. 200 μL were collected in 0.5 mL K3-EDTA (Sarstedt, Germany) tubes after fasting for 12 hrs. The plasma fraction was isolated by immediate cold centrifugation and frozen for banking. Urine volume excretion in 12 hrs. was measured, aliquoted in 1.5 mL Eppendorf tubes and frozen for further analysis. Albumin excretion in urine was measured by an indirect competitive ELISA method developed by the "Zentrum für Medizinische Forschung". Hyperglycemia was assessed in a drop of raw blood by glycated hemoglobin analysis (clover HbA1c analyzer on hADSC cohort and A1cNow+ monitoring kit in cohort ABCB5+) or fasting plasma glucose with a OneTouch Verio IQ meter.

Tissues were fixed *ex vivo* by retrograde perfusion as follows: mice were anesthetized by intraperitoneal injection of a cocktail of Ketamine (Wirtschaftsgenossenschaft deutscher Tierärzte eG, Germany) and Xylazine (Serumwerk Bernburg, Germany) in a ratio of 3:0.05 mg per 10 g BW. A mid-abdominal incision was performed in the absence of toe withdrawal reflex, the abdominal cavity was organized and the left renal artery clamped for kidney isolation

and immediate cryopreservation. Next, the abdominal aorta was cleaned, isolated and cannulated below the renal bifurcation with a G21 winged infusion set connected by a 3-stage valve to a compressor pump (4% paraformaldehyde or heparinized saline solution delivery) and a piston syringe pump (dye delivery). The tip of the G21 set was clamped facing upwards (retrograde perfusion) and the cava vein ruptured. Heparinized saline solution was perfused at 200 mbar for 6 minutes. Right after, a 1 mg/mL solution of MHI148-PEI in phosphate buffer-saline was perfused via piston pump at 1 ml/min rate for 10 minutes. Next, heparinized saline solution was perfused for 1 min to rinse the remaining fluorescent dye. Then, 4% paraformaldehyde solution was perfused for 6 minutes. Kidney, pancreas, heart and aorta were collected and incubated in dark conditions for 18 hours in a 4% paraformaldehyde solution. Finally, tissue was processed for paraffin inclusion or tissue clearing.

5. Tissue processing

5.1.   Tissue clearing and fluorescent staining: an overview

Light scattering is a physical phenomenon that explains opacity and transparency in nature. While living tissues present high scattering properties that makes them opaque, glass for example presents little scatter, which is perceived as transparency. Tissue clearing protocols aim to reduce light scattering phenomena (i.e. light refraction) from living tissues by minimizing their interaction with light, thus increasing their transparency. Refraction is a particularly important light scattering event that affects tissues due to their molecular heterogeneity (e.g. lipids, water, proteins, etc.), and the main target of tissue clearing protocols. Using the previous example, glass can be several centimeters thick, but preserves its transparency due to its structural uniformity, while a few millimeters of tissue are fully opaque. Following the same principle, tissue clearing increases transparency by elimination of refractive index disparities caused by different molecules in cells. A full description of the principles of tissue clearing have been excellently reviewed by Richardson et al., (2015) [45]. The protocol used in this work was a solvent-based clearing approach that dehydrates and washes away the lipid content from the sample, increasing homogenization.

Full-transparency and opacity are two extreme situations that are not desirable in microscopy. The fundaments of histology and bright field microscopes lays on the slight refraction of light after interacting with a slice of tissue, thus making structures visible. In the same way, transparency hampers the interpretation of tissue

structures. Under this rationale, tissue clearing protocols need to be also compatible with staining agents to increase contrast without losing transparency. This is an often-neglected key factor of tissue clearing: that not only depends on the clearing approach, but also the correct selection of dye (typically a fluorescent one) and the suitable microscope for digital analysis. The dye employed in this work was MHI148-PEI: a highly cationic molecule covalently attached to the fluorophore Cy7. Although perfusion staining with MHI148-PEI is an unspecific chemical dyeing strategy, it enables the specific staining of the vascular tree due to its ionic interaction with the negatively charged glycocalix of the endothelium. As a result, vessels can be visualized in cleared kidneys in the red/infrared electromagnetic spectra with dark field microscopes.

5.2.   Ethyl-cinnamate clearing

Perfused organs with MHI148-PEI were cleared with the organic solvent ethyl-cinnamate (Sigma, Germany) as described in [90] using an automated tissue processor (TP1020, Leica microsystems, Germany). Shortly, full organs were dehydrated by using an ethanol gradient of 50%, 80%, 100% and 100% once more for 30 minutes each at 37°C. Afterwards, the sample was submerged in ethyl-cinnamate overnight. The cleared kidney was stored right after in ethyl-cinnamate in an opaque 15 mL tube until imaging (Eppendorf, Germany).

5.3.   Paraffin inclusion and PAS staining

Full or half organs were incubated two times in fresh 4% paraformaldehyde, dehydrated with an ethanol gradient of [70%, 80%, 96%, 99% and 99%], incubated in Xylol two times, and finally embedded in liquid paraffin in three steps (1.5 hrs. each). All steps were performed using the above-mentioned tissue processor. Slices of 3-µm thickness were cut from kidneys onto glass slides using a rotary microtome (Richert-Jung Biocut 2030, Leica microsystems, Germany).

Slices were deparaffinized in Xylol and rehydrated for staining with a conventional PAS method. Shortly, periodic acid solution was added to the slides, incubated with Schiff's reagent and stained after with hematoxylin. Between each step, slides were thoroughly rinsed with distilled water. The slides were dehydrated with an alcohol gradient and Xylol as indicated before, and preserved in mounting medium.

6. Dark field microscopy

6.1.   Overview of three-dimensional analysis by dark field microscopy

Dark field microscopy makes use of fluorescence-emitting molecules to visualize structures in tissues using lasers instead of "bright" light for imaging. The advantages over bright field microscopes are the selective illumination of several structures of interest by laser excitation on fluorophores, and the possibility to split the detected fluorescence in independent illumination channels for further analysis. Yet, regular dark field microscopes are only useful for two-dimensional purposes. Advanced microscopes such as confocal and light sheet have an additional level of complexity, which is to exclude out-of-focus fluorescence for semi-quantitative and highly specific scanning purposes. Although fluorescence is already a semi-specific imaging strategy, regular dark field microscopes cannot image single focal planes independently in samples (also known as optical sectioning). Optical sectioning can be described as an image that does not receive information from upper or lower optical planes, often perceived as "bright blurring" in bright field and in regular dark field microscopes. The possibility of true single focal planes scanning enables three-dimensional analysis by the stacking of optical sections at different levels in the Z-axis of the sample. As a result, a real three-dimensional aspect of objects can be obtained by digital reconstruction. Two of the most popular three-dimensional reconstructions are volume (interpolation of sequential optical sections to simulate a continuum), or orthogonal projections (eagle-view of stacked single focal planes).

As mentioned earlier, confocal and light sheet microscopes are two different and complementary approaches for three-dimensional analysis that allows optical sectioning. Confocal microscopes do single point scanning in the XYZ space of a sample by epifluorescence stimulation and single particle detection. This approach consists in "vertical" pulsed stimulations on the surface of the sample releasing a single photon that is detected by electromagnetic detectors and immediately reconstructed as a three-dimensional pixel (voxel) of a full image. Instead, light sheet microscopes perform horizontal stimulation of a sample in the Z-axis and image acquisition by digital cameras placed in the orthogonal position. A comparative description of both strategies used in this work is summarized in Table 3. A light sheet microscope was employed in this work over confocal for three-dimensional analysis due to its rapid acquisition and better Z-resolution. A confocal microscope

was employed instead for two-dimensional analysis due to its excellent XY resolution and robust sensitivity to detect red/infrared fluorescence.

Table 3 – Comparative key parameters between confocal and light sheet microscopes

Key parameters	Confocal microscope – TCS SP8	Light sheet microscope – DLS TCS SP8
XY resolution	High	Medium
Z resolution	Medium	High
Speed acquisition	Slow	Fast
Data volume acquisition	Medium	High
Z effective scanning	Medium	High
Optical sectioning strategy	Single-point scanning by epifluorescence stimulation	Double light sheet horizontal stimulation
Wavelength detection strategy	Acousto-optic tunable filter (AOTF)	Filters
Signal to background ratio	High	Low
Image acquisition	Single particle detection by photomultipliers	Digital monochromic camera

6.2.   Three-dimensional microscopy settings

Cleared kidney portions of 1-2 mm thickness (3-5 mm height) were prepared and stuck on top of a 0.5 mm Parafilm folded base, glued to a Ø-35 mm glass bottom dish. Samples were imaged with a double light sheet microscope (DLS TCS SP8, Leica microsystems), with a 1.6x illumination objective and a 5x solvent-resistance detection objective + 7.8 mm mirror cap. Ethyl-cinnamate was used as immersion media (refractive index=1.56).

Excitation lasers (552 nm and 638 nm wavelength, respectively) were used for fluorescence emission in green/yellow (auto fluorescence peak) and red/far-red (MHI148-PEI peak) range of spectra. Images were taken at maximum pixel resolution (2048x2048) and 1.44 µm Z-step size (voxel final size 0.718x0.718x1.44 µm).

6.3.   Image analysis: Feret's diameter

Image acquisition and preparation of three-dimensional pictures were performed using Leica Application Suite X (LASX v.3.5.6, Leica microsystems). Standard optical subsets of 1 mm^3 were cropped from full raw scans and exported as independent channels in .TIFF format for analysis. Three standard optical subsets representing pole, mid-pole and center portions of the same kidney were used for the analysis. Image processing was performed using FIJI (ImageJ 1.52p) on the MHI148-PEI channel of the standard optical subsets as follows: [background subtraction=20] > [2x2 maximum fluorescent binning] > [Gaussian blur filter σ=3] > [Minimum filter=5] > [Maximum filter=5] and exported as .HDF5 format. Subsequently, images were segmented with Ilastik (v1.3.2) with a trained classification for vessels, background and glomeruli. Segmented files were exported as simple segmentation .HDF5 files. Glomerular parameters were assessed by using the ImageJ apps: 3D Objects Counter [91] and 3D ImageJ Suite (3DSuite) [92] on segmented files.

6.4.   Image analysis: afferent arteriole diameter

Ten visible afferent arterioles with their corresponding glomerular tuft were randomly selected from each of the 1mm^3 standard optical subsets of three mice from each group. Unlike in the previous analysis, maximum arteriolar diameter was established by selecting the optical section with the largest observable distance in XY closer to the tuft.

6.5.   Two-dimensional microscopy settings

Paraffin sections were imaged right after slicing with a confocal microscope (TCSP8, Leica microsystems), with a 10x objective at medium pixel resolution (512x512). Excitation lasers (488 nm and 638 nm wavelength, respectively) were used for fluorescence emission in green/yellow (auto fluorescence peak) and red/far-red

(MHI148-PEI peak) range of spectra. Same slices were scanned after PAS staining with a slide scanner (Aperio VERSA, Leica microsystems) with a 20x objective.

6.6.   Image histological analysis

Image acquisition was performed using LASX. Fluorescent images processing was performed using FIJI by subsetting 10 random glomeruli of a random slice per mice. The same subset was identified in PAS images for comparison.

7. Statistical analysis

Continuous variables were expressed as means plus/minus their standard deviation (SD) or standard error of the mean (SEM) when performing estimates, or least squared means (LSM) plus/minus standard error (SE) when data was analyzed by repeated-measures ANOVA. Normally distributed variables were analyzed with student's t-test for two independent groups or ANOVA for multiple groups at single time-point comparisons with Levene's post-hoc test. Mixed-factor repeated measures ANOVA with Tukey's HSD as post-hoc test was applied for longitudinal assays between two groups. Bivariate analysis was performed to evaluate correlation between continuous variables (i.e. glomerular size and afferent arteriole's diameter). The Log-rank test was used to evaluate differences between non-parametric variables. All analyses were performed with JMP (v.15.0.0).

3. Results

1. Physiological parameters

1.1.   Baseline parameters

Two cohorts of BTBR$^{ob/ob}$ mice were studied, each with a randomized obese (OB) treated and control group. In both cohorts and in both groups, mice presented profound hyperglycemia (Figure 3) and albuminuria (Figure 4) at 11 weeks of age before the beginning of intervention. Values of hyperglycemia were higher in cohort hABCB5+ as already at 11 weeks of age almost 50% of the mice had HbA1c levels above the detection limit (>13%). It is worth mentioning that, due to the discontinuation in the production of cartridges used for HbA1c determination before the experiments conducted in cohort hABC5+, glycation had to be determined by an alternative device.
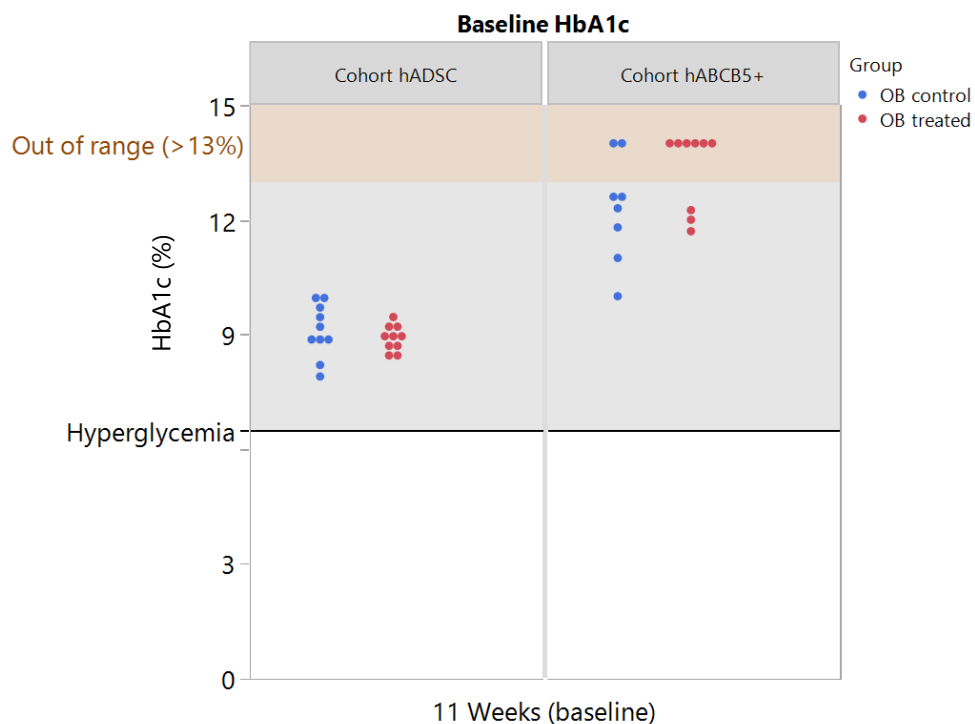
Figure 3 – Baseline HbA1c levels in BTBR$^{ob/ob}$. Hyperglycemia (>6.5% grey-colored area) was observed at 11 weeks of age in all groups. Cohort hABCB5+ (N$_{control}$ = 9, N$_{treated}$ = 10) presented higher glycation levels with eight mice above the detection limit (orange-colored area) compared to cohort hADSC (N$_{control}$ = N$_{treated}$ = 10).
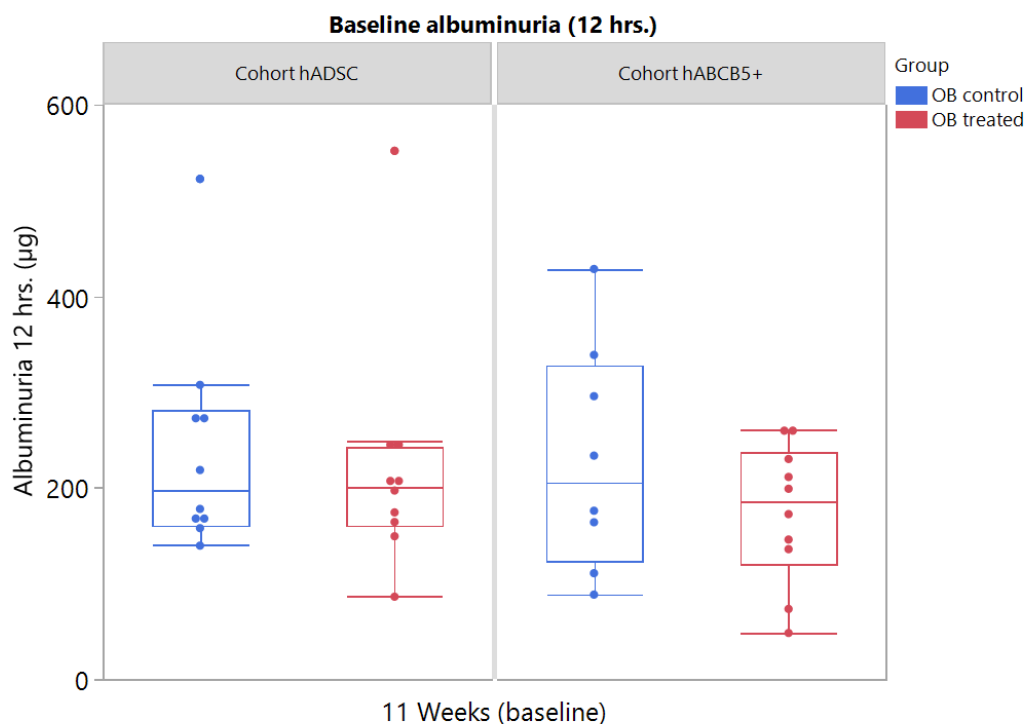
Figure 4 – Baseline albuminuria levels in BTBR$^{ob/ob}$. Albumin concentrations were measured by ELISA and multiplied with the volume of urine collected in 12 hrs. Cohort hADSC (N$_{control}$ = N$_{treated}$ = 10) and cohort hABCB5+ (N$_{control}$ = 8, N$_{treated}$ = 10) presented similar albuminuria values.

1.2.   Survival

Similar to the extent of hyperglycemia, mortality was significantly higher in the hABCB5+ cohort as 10 out of 20 mice had to be sacrificed or died spontaneously, while in cohort hADSC only four reached composite endpoints (Figure 5). Death by embolism due to MSC infusion was not observed in both treated groups. Treatment with MSC did not improve survival.

A retrospective hygiene analysis on plasma samples of cohort hADSC showed that 80% of the mice were infected by mouse parvovirus. This however had no impact on their survival.

Euthanized mice and those that died spontaneously frequently showed abnormal macroscopic structures such as cysts in kidneys and other organs, tumors in the abdominal cavity, deposition of white solid material, and sometimes bladder occlusion (data not shown). Additionally, at least 20% of the diabetic mice (irrespective of group and cohort) presented such abnormalities in a single kidney with normal appearance of the contralateral one (Figure 6).
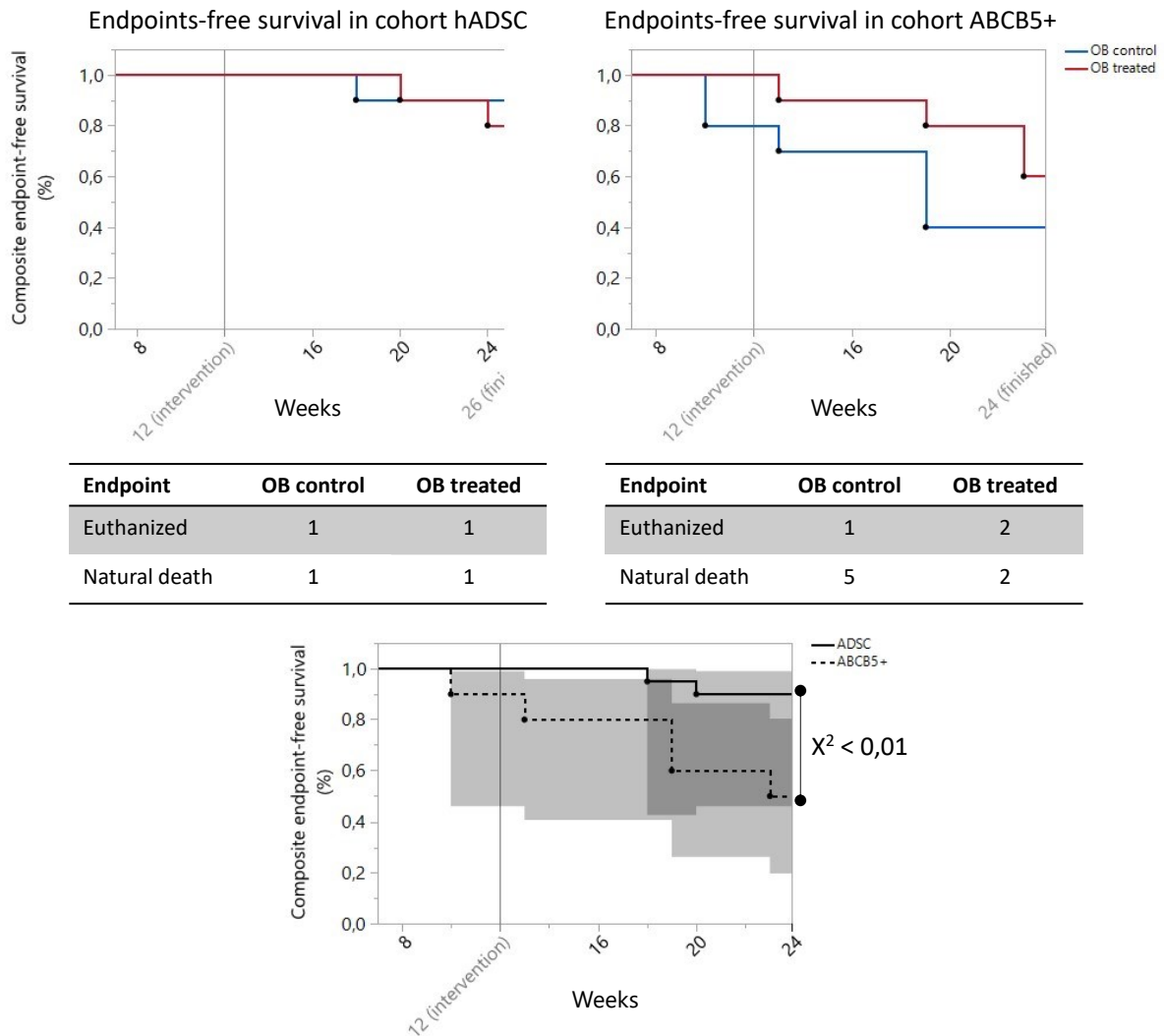
Figure 5 – Experimental endpoints-free survival. OB control and OB treated groups did not show significant differences in survivors (hADSC: $n_{control}$ = 8, $n_{treated}$ = 8; hABCB5+: $n_{control}$ = 6, $n_{treated}$ = 4). Mice with high severity score were euthanized during the experiment according to animal welfare and legislation. Survival rate was significantly higher in cohort hADSC than hABCB5+ (X^2 < 0.01, grey area: 95% confidence interval).

Figure 6 – Single kidney lesions in diabetic mice. Representative images of a set of kidneys recovered from the same mouse. Lesions were present in different degrees in mice irrespective of group and cohort.

1.3.   Longitudinal hyperglycemia and albuminuria

Intervention with MSC did not mitigate hyperglycemia in two independent cohorts although in some of the treated mice HbA1c dropped more than 2% (Figure 7). Groups from cohort hADSC did not experience a significant increase in HbA1c levels after 12 weeks. Statistical analysis could not be performed in cohort hABCB5+ due to glycation levels beyond the detection limit.
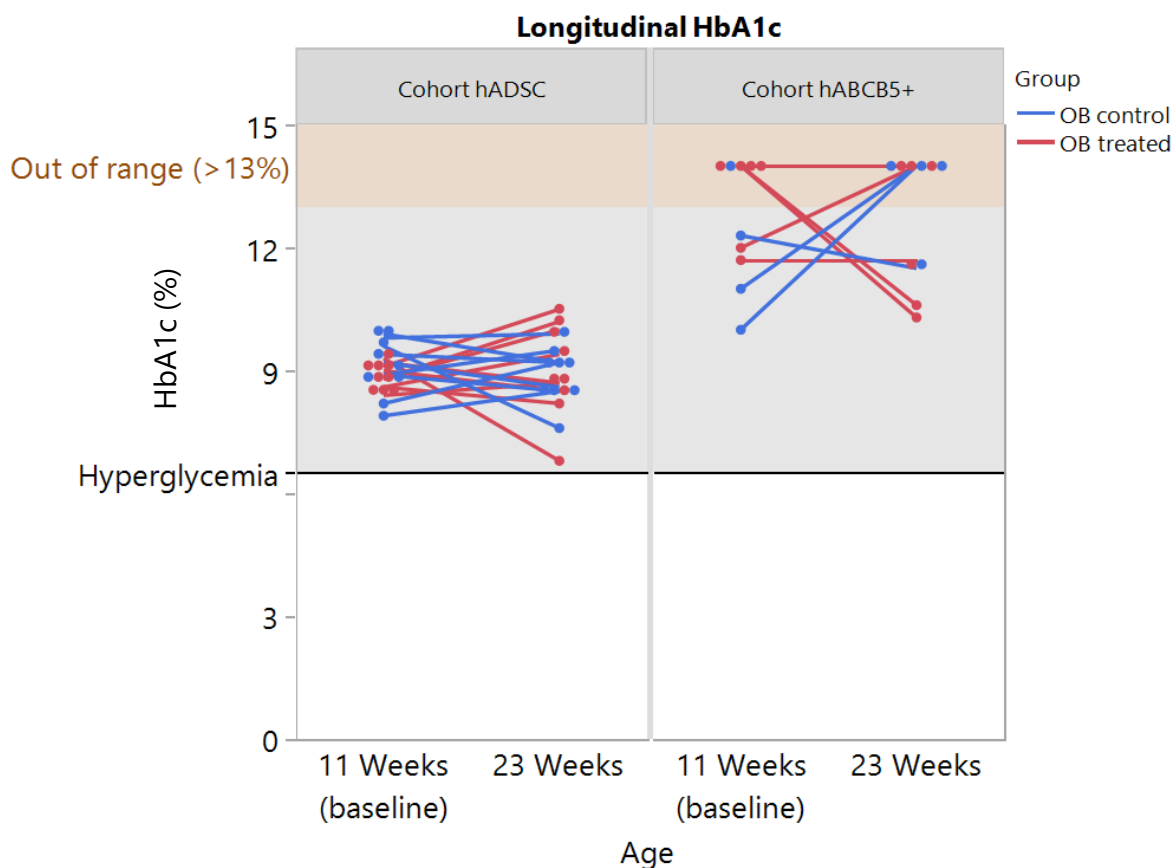
Figure 7 – HbA1c levels in the course of disease. Comparative levels of HbA1c before treatment (data presented in Figure 3) and twelve weeks after. Lines (blue: OB control mice, red: OB treated mice) represent the trend between two separate measures before and after treatment with MSC (hADSC: $n_{control}$ = 8, $n_{treated}$ = 8; hABCB5+: $n_{control}$ = 6, $n_{treated}$ = 4). Orange-colored area: above detection limit, gray-colored area: hyperglycemia. Mice with single measurements were excluded.

Treated mice presented lower albuminuria values after treatment induction at 11 weeks in cohort hADSC. This trend was not observed at 23 weeks of age, in which albuminuria reached similar levels as control (Figure 8). In cohort hABCB5+, treated mice also exhibited lower values during the experiment after treatment. Statistical analysis of albuminuria was carried out following mixed-factors ANOVA for repeated measures with age and group as fixed factors. Mice differences were considered as

a random factor to compensate the variation associated to: mice's independent course of albuminuria with age, and mice exclusion due to composite endpoints met. Twelve-hour albuminuria did not significantly differ between age-matched treated mice and their respective controls in both cohorts. Although non-significant, OB treated groups in both cohorts showed similar trends in reducing albuminuria.
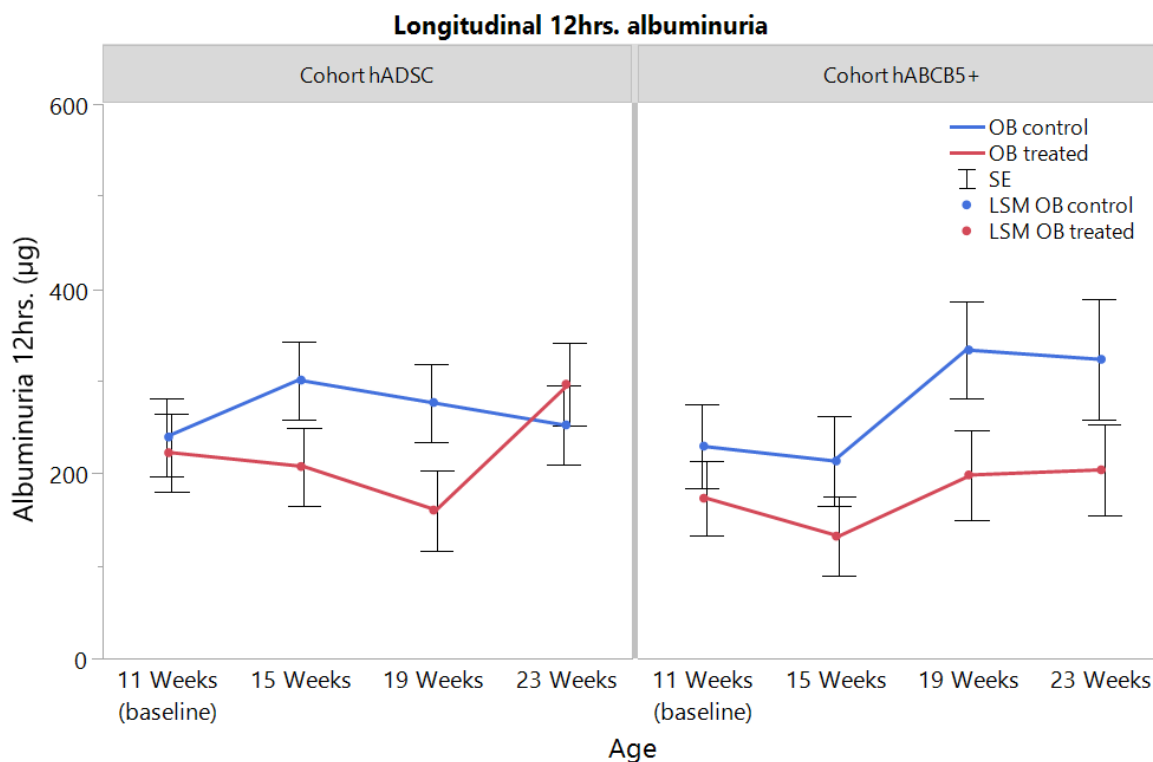
Figure 8 – Albuminuria in the course of the disease. Treatment with MSC (red line) did not show a significant improvement in 12 hours albumin excretion compared to control (blue) either in cohort hADSC (left) or hABCB5+ (right). LSM: least square mean. SE: standard error.

1.4. GFR

Half-life time clearance of FITC-sinistrin did not differ in the groups of cohort hADSC at 24 weeks of age (Figure 9). Earlier time points were included in cohort ABCB5+ in order to evaluate possible hyperfiltration events. Still, diabetic mice did not differ in clearance at 17 weeks of age, nor in association to age-matched wild-type mice included at 21 weeks. Converted clearance values to GFR (normalized by BW as described in Eq. 1) did not show evidence of hyperfiltration or renal impairment as well when compared with age-matched wild-type mice (Table 4).
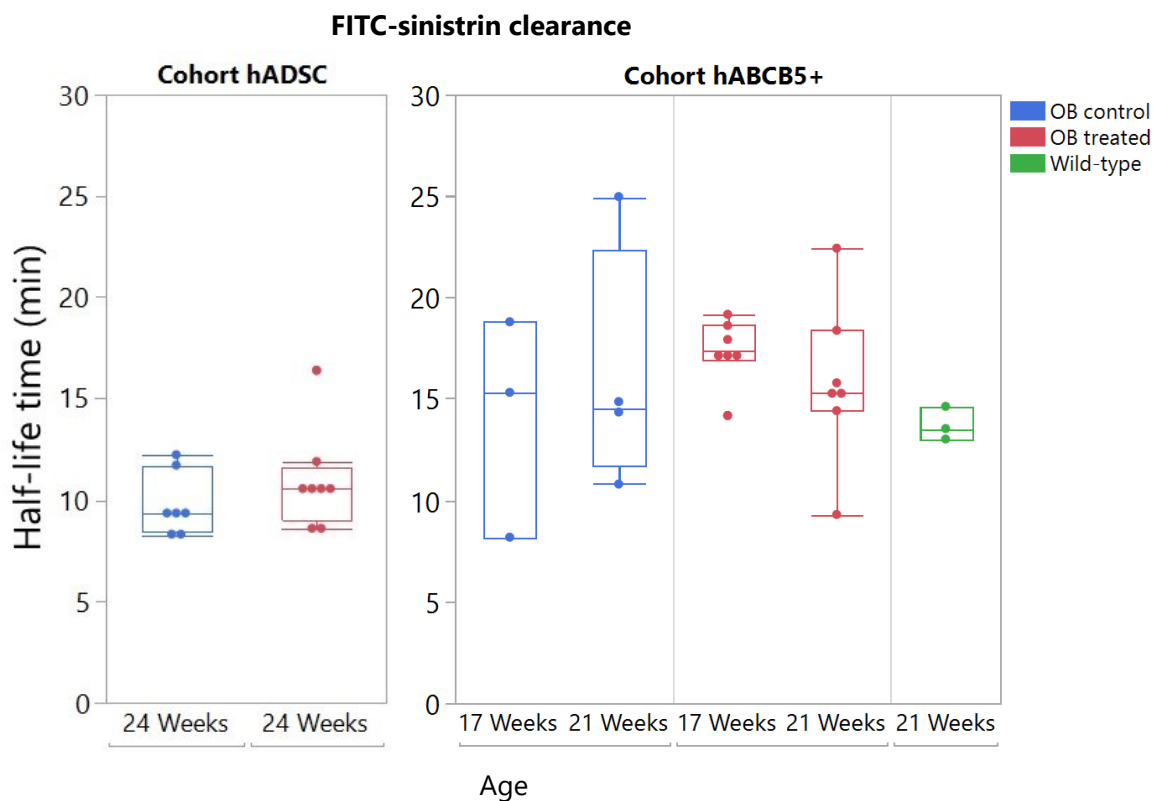
Figure 9 - Half-life time clearance of FITC-sinistrin in mice. Mice treated with MSC (red) showed similar values of clearance at 24, 21 and 17 weeks of age compared to their controls (blue). No differences in clearance were also observed when comparing diabetic mice with wild-type phenotypes at week 21 (green).

Table 4 – GFR normalized by body weight

Experiment	Age (weeks)	Group	Mean ± SD (ml/min)
Cohort hADSC	24	OB control	0.98 ± 0.24
		OB treated	0.94 ± 0.20
Cohort ABCB5+	17	OB control	0.69 ± 0.27
		OB treated	0.54 ± 0.05
	21	OB control	0.56 ± 0.15
		OB treated	0.66 ± 0.20
		Wild-type	0.41 ± 0.05

2. Histology

2.1.   Histopathologic comparison in PAS-stained sections

Kidney sections stained with PAS from treated and untreated diabetic mice presented mild to marked diffuse mesangial expansion when compared to wild-type kidneys. Glomerulosclerotic lesions (partial or total) were also noticeable in diabetic mice, along with increased glomerular tuft size. At least 10% of diabetic mice from both cohorts presented hydronephrosis characterized by dilation of the renal pelvis. Treatment with MSC in both cohorts did not show a distinctive overall reduction of glomerular lesions or discernible aggravation in kidney histology (data not shown).

2.2.   Tissue clearing implementation

Previous experiments conducted in our group showed a significant enlargement of the glomerular tuft in kidney sections of diabetic BTBR mice compared to their healthy littermates [93]. In the present study, we performed tissue clearing and three-dimensional analysis to quantify with a semi-automated approach the enlargement of the glomerular tuft and additional features of DKD. As a first step for validation, a pipeline was developed to analyse the maximum glomerular diameter (Feret's diameter) in a three-dimensional space of a large number of glomeruli in optical sections of cleared kidneys.

Optical sections from diabetic kidneys displayed glomerular enlargement when compared with age-matched non-diabetic mice (Figure 10). To confirm this observation in a reliable and quantitative manner, Feret's diameter of all identified glomeruli in standard optical subsets of 1000 μm^3 was assessed with a semi-automated methodology. The pipeline summarized in Figure 11 was developed to segment all glomeruli in random standard optical subsets from scanned portions of a kidney. Validation of the segmented glomeruli took place by comparing the identified regions of interest by the pipeline (in this case, the glomeruli) with the original raw data acquired by the microscope (combined signal emitted by the autofluorescence of the sample and MHI148-PEI fluorescence). Wild-type kidneys showed a high level of correlation between regions of interest and raw images (Figure 11 B-3). Non-valid glomeruli were also recognized as regions of interest in the segmented file due to misclassification of brightly stained vessels, and indivisible units such as side-by-side glomeruli, or glomeruli attached to different vessels. In contrast, diabetic kidneys had

a much larger rate of non-valid glomeruli due to increased compactness (much higher rate of side-by-side glomeruli), and notably, misperfused glomeruli. An interesting aspect that will be discussed in more detail later in this section.

Feret's diameter of identified glomeruli in wild-type and diabetic mice showed normal distributions that were comparatively different between the two groups (Figure 11, C).
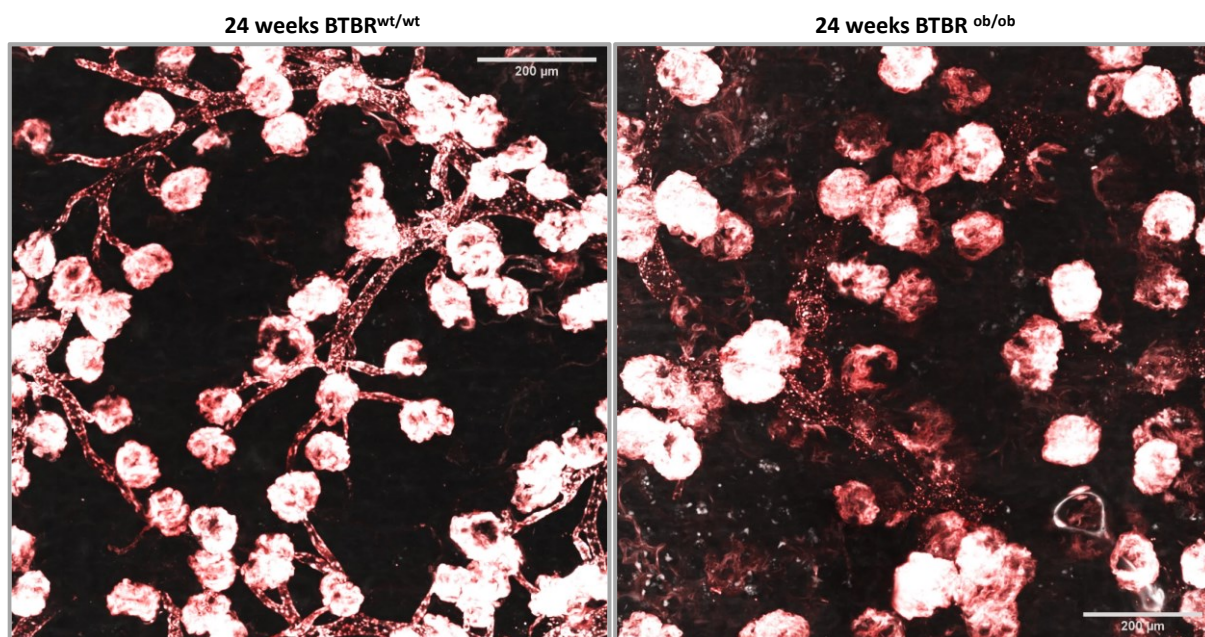
24 weeks BTBR$^{wt/wt}$ **24 weeks BTBR $^{ob/ob}$**

Figure 10 - Maximum projection of cleared kidneys. Mice kidney portions previously perfused with MHI148-PEI (red). The maximum projection (that is, an orthogonal representation of a stack of optical sections into one single image) depicts 1 mm-thick stacked sections (695 optical sections into one single image). The glomerular size of diabetic kidneys is substantially larger compared to wild- type mice (scale bar: 200µm).

A
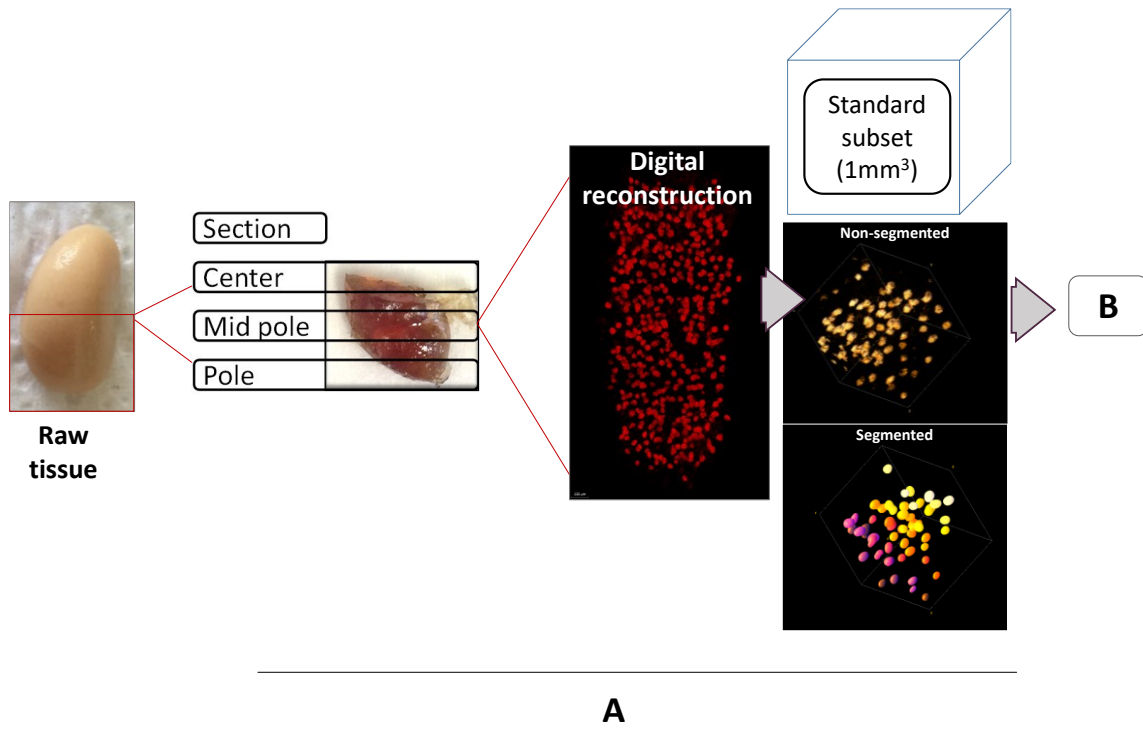
Figure 11 – Workflow of morphometric analysis and pipeline of semi-automated segmentation in the kidney. After clearing and imaging of a thick kidney portion (A), the stack of images is cropped in random 1mm³ standard optical subsets.
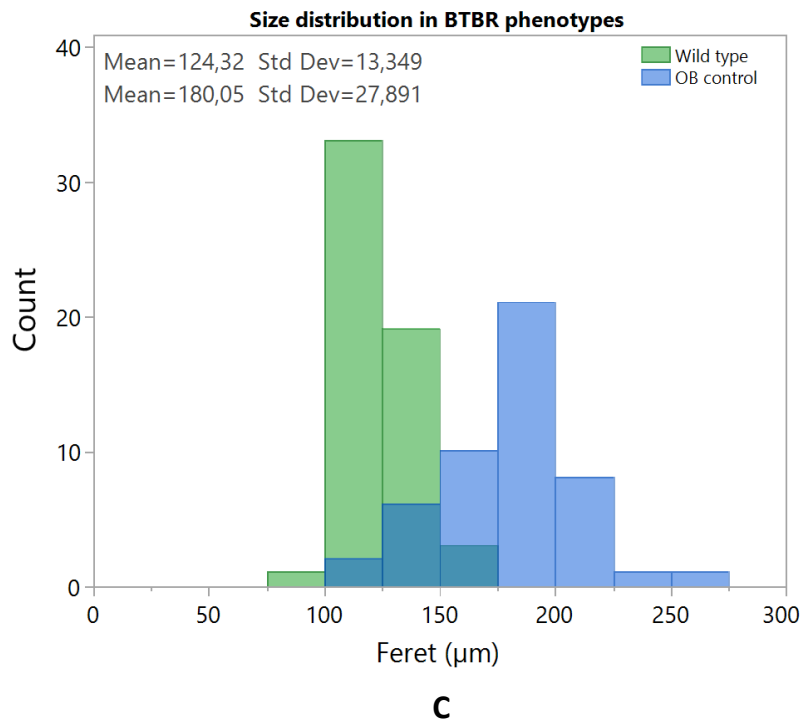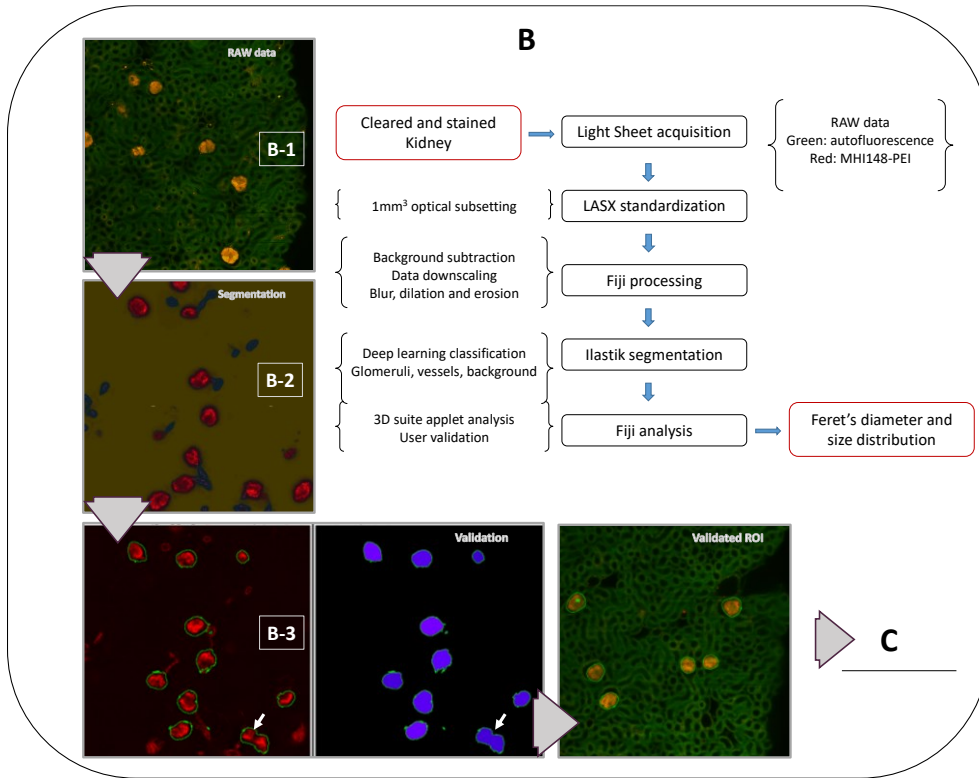
(cont. 11) RAW data subsets are exported as .TIFF files and pre-processed with FIJI (B-1). A deep learning approach using Ilastik was employed by classifying pixels corresponding to glomeruli (red), background (yellow) and vessels (blue) (B-2). Segmented regions of interest are later exported back to FIJI, and analyzed with the package tools 3D suite. A validation step is performed afterwards by comparing regions of interest with the MHI148-PEI and autofluorescence channels before analysis (B-3). Each region of interest is later analyzed and the morphometric parameters extracted from the digital reconstruction (C).

2.3.   Glomerular size distribution

Cleared kidneys from wild-type, and diabetic mice from cohort hABCB5+ were analyzed for glomerular size distribution following the pipeline described above. Standard optical subsets from pole, mid-pole and center were measured for all cleared kidneys (Figure 12). Glomeruli analyzed from these three sections displayed a similar size distribution with no significant differences within kidney. Therefore, Feret's diameter values were pooled for each mouse with their corresponding numerical weight from the overall group (N/N_{group}). Treated diabetic mice had a significant glomerular enlargement compared to wild-type (Figure 13). OB control mice did not reach significancy (*p-value* = 0.06), although enlargement is evident. None of the cohort's OB treated groups differed from OB controls in this aspect.
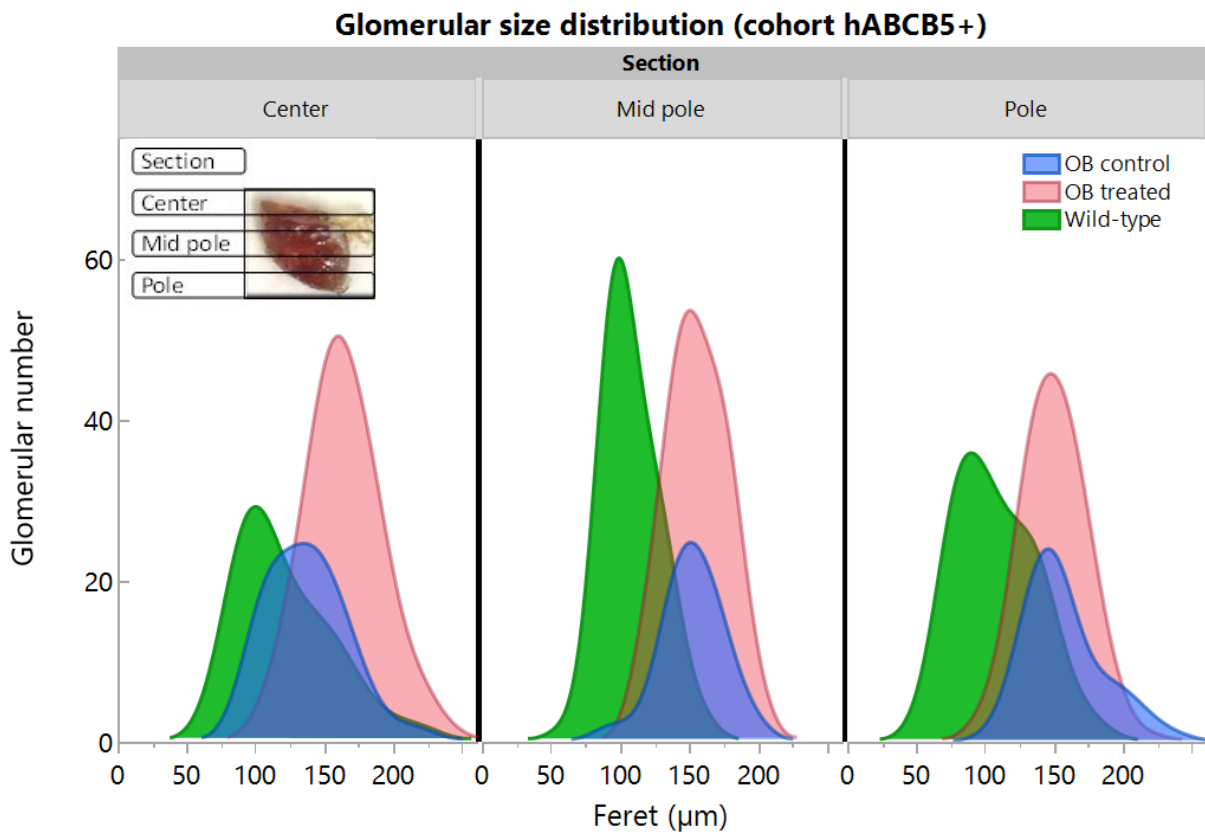
Figure 12 – Glomerular size distribution in cohort hABCB5+. Histograms of glomerular size distribution in three different portions of the kidney (center, mid pole and pole). Valid glomeruli count and average distribution did not differ significantly among the studied sections (n=3, all groups).
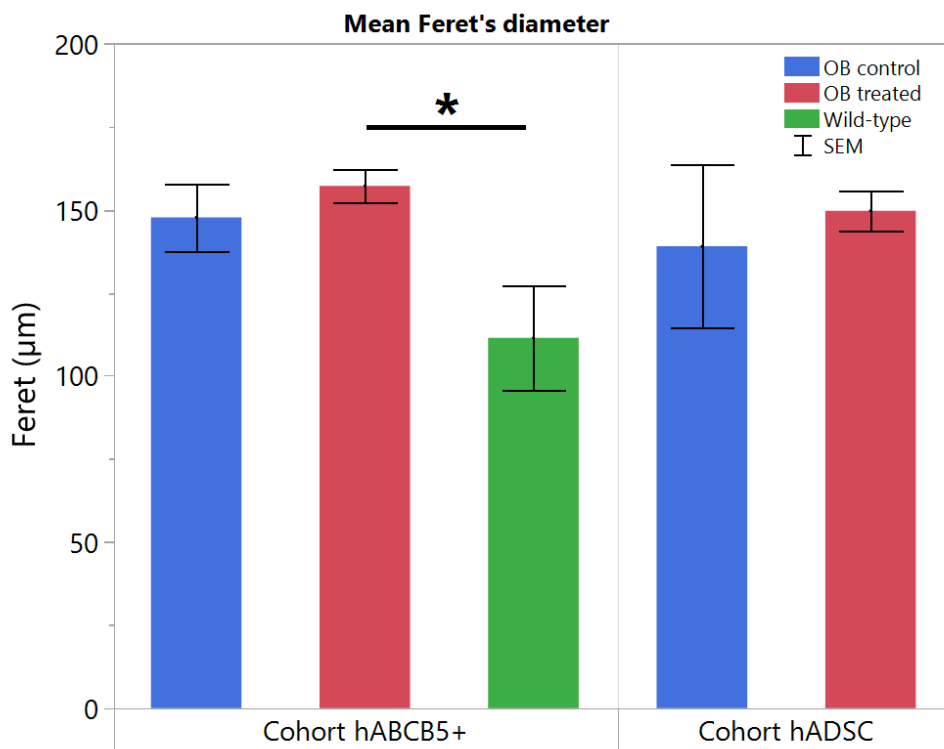
Figure 13 – Glomerular mean size per experimental group. Feret's diameter of diabetic phenotypes differs significantly compared to lean mice. No statistical differences were observed between diabetic mice in the two independent experiments (cohort ABCB5+ $n_{wild-type}$=3, $n_{control}$=3, $n_{treated}$=6; $F > 0.05$, *p-value < 0.05; cohort ADSC n=2). SEM: standard error of the mean.

2.4. Afferent arteriole analysis

Tissue clearing data were also used for analysis of the diameters of afferent arterioles. To this end, the diameter of the afferent arteriole as illustrated in Figure 14 was measured in ten random glomeruli of wild-type, OB control and ABCB5+ treated OB mice (n=3 for all groups). The mean diameter of the afferent arteriole in diabetic mice was significantly larger compared to wild-type mice, but did not differ between treated and control diabetic mice. Efferent arterioles were seldom visible in all standard optical subsets because of the low signal to background fluorescence intensity ratio, making them unable to measure with this approach. Therefore, quantitative analysis could not be conducted as described above. A higher number of efferent arterioles could be visible in the original data as depicted in Figure 15. A qualitative comparison between afferent and efferent arterioles on the same glomeruli indicates a large diameter in the afferent and reduced diameter in the efferent portion of diabetic mice. This large difference between dilation of the arterioles was not observed in kidneys of lean mice.
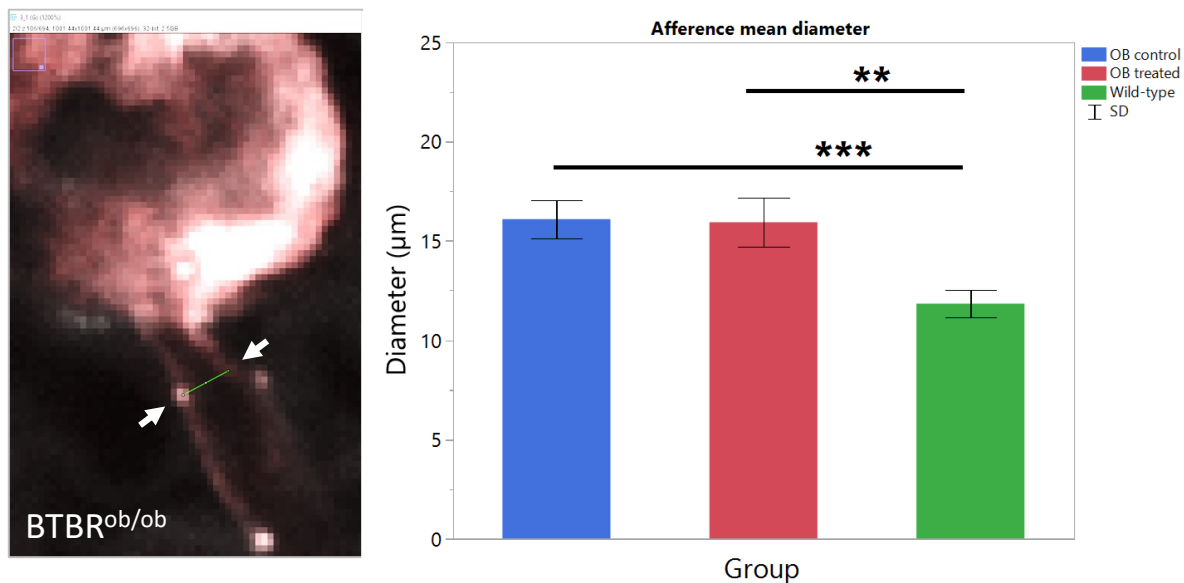
Figure 14 – Afferent arteriole diameter in cohort ABCB5+. The afferent arteriole of ten random validated glomeruli by our pipeline was measured as shown on the left picture. Representative optical sections for each afferent arteriole were selected to measure its maximum diameter (white arrows). Wild-type mice presented significant differences when compared to diabetic mice as shown on the right graph (n=3; **p-value < 0.01; ***p-value < 0.001).
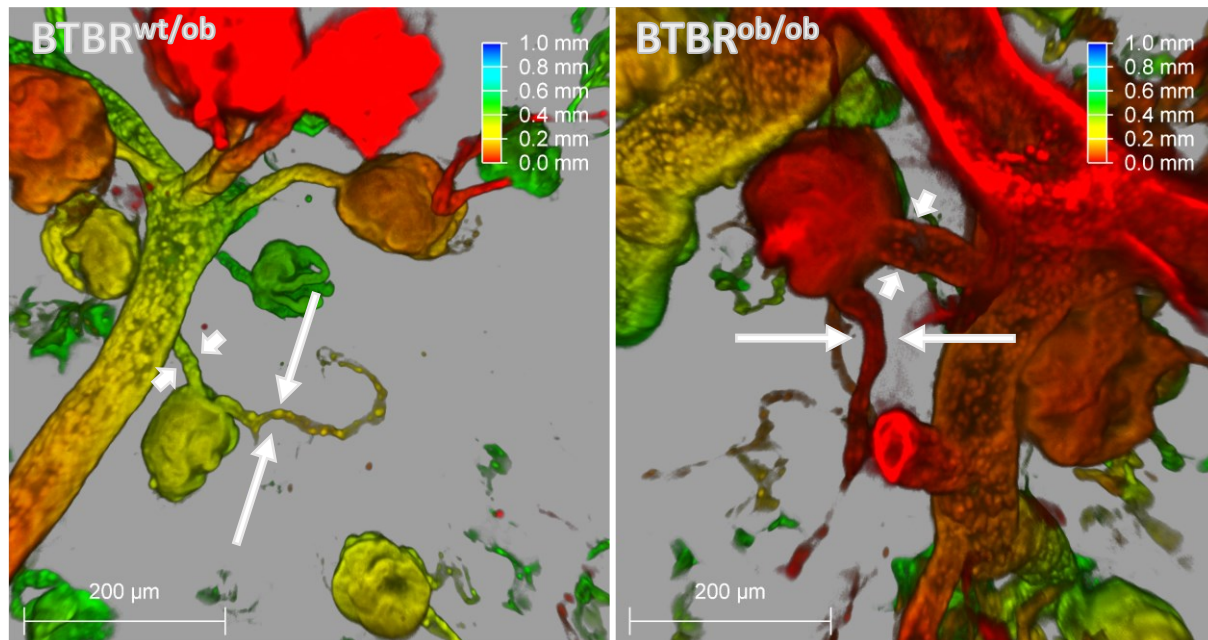

Figure 15 – Three-dimensional aspect of afferent (short arrows) and efferent arterioles (long arrows) in the BTBR mice. Wild-type phenotypes (left) present less dilated afferent arteriole when compared to diabetic mice (right). Seemingly, efferent arterioles have a higher constriction in diabetic mice. Scale bar: 200 μm. Color-coded image to improve depth perception from red (closer) to blue (farther).

2.5.   Arteriolar cross-sectional diameter and glomerular size

Each estimated arteriolar size used in the previous analysis was correlated with its respective Feret's diameter. An overall positive correlation was found between afferent diameter and glomerular size irrespective of group (Figure 16). OB control values followed a significant positive correlation like the one observed in the general tendency (*p-value* < 0.05). Contrarily, wild-type and OB treated group's dispersion could not be explained by this interaction.
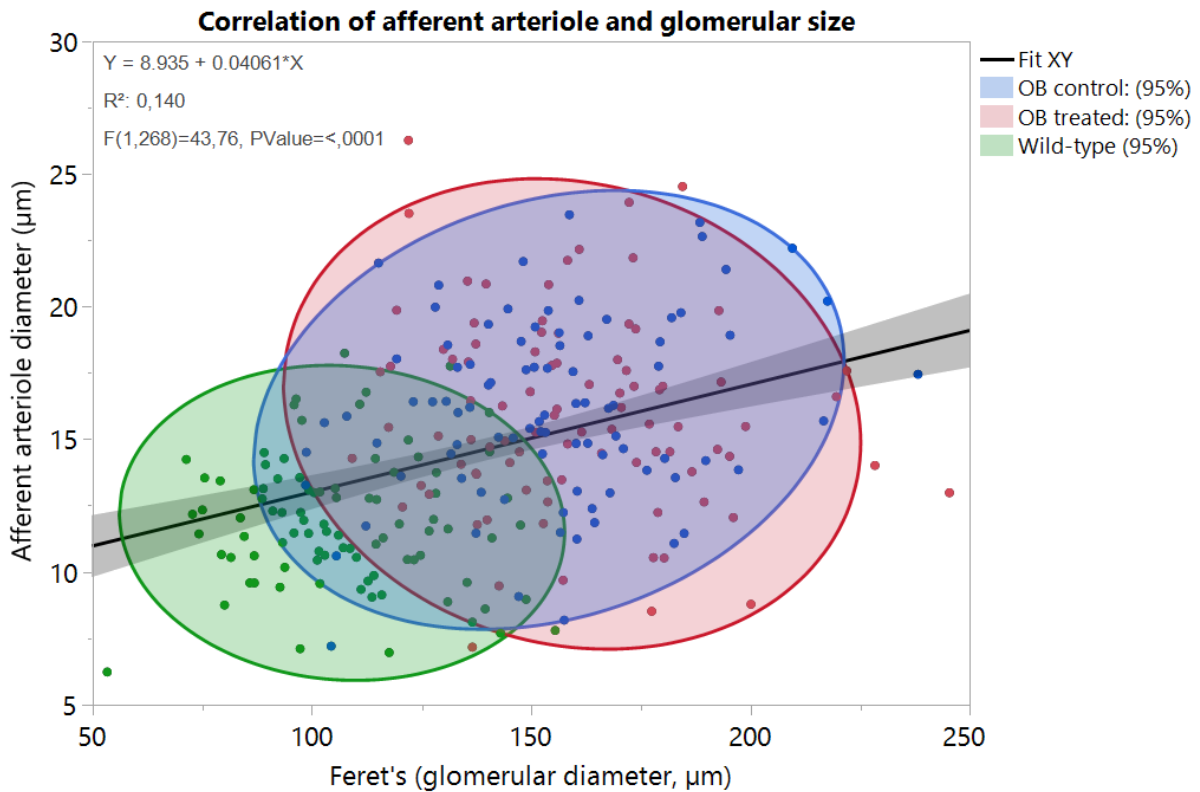
Figure 16 – Bivariate correlation between afferent diameter and glomerular size. Each dot represents the paired observation between Feret's diameter (X-axis), and the diameter of its afferent arteriole (Y-axis). Thirty glomeruli were measured per mouse (n = 3, all groups). An overall positive linear correlation is observed between the two variables (black line). Shadowed areas represent the 95% confidence interval of wild-type (green), OB control (blue), OB treated (red) or all data (grey).

2.6.   Perfusion pattern in diabetic mice

As mentioned earlier in this section, a high incidence of misperfused glomeruli were repeatedly observed in BTBR$^{ob/ob}$ mice when applying the tissue clearing methodology. An overview of large scanned sections of healthy vs. diabetic mice (Figure 17 & Figure 18, respectively) shows glomeruli with a round and almost spherical shape in wild-type, while open and hollow-centered in most of cases in diabetic mice. We qualified these differences by assigning each glomerulus to one of the following classes: "valid glomerulus" (correctly identified by our pipeline and included in our morphometric analysis of size distribution and afferent dilation), "false negative" glomerulus (fully perfused but discarded by fusion with other close structures or not recognized by the algorithm), and "half or non-perfused" glomerulus. Mean total number of glomeruli, and the maximum and minimum percentages of glomeruli for each class were estimated as depicted in Table 5.
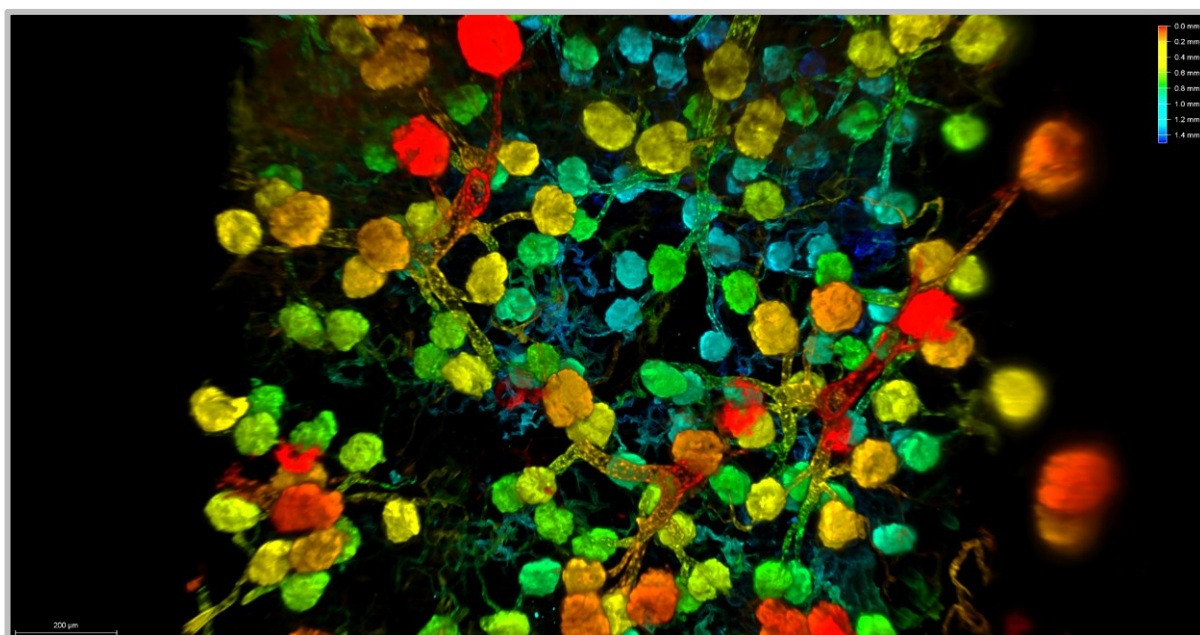

Figure 17 – Overview of a kidney section from a wild-type mouse. Vascular tree and glomeruli are visible in a 1.5 mm thick section. Orthogonal view from a three-dimensional reconstruction. Color-coded image to improve depth perception from red (closer) to blue (farther).
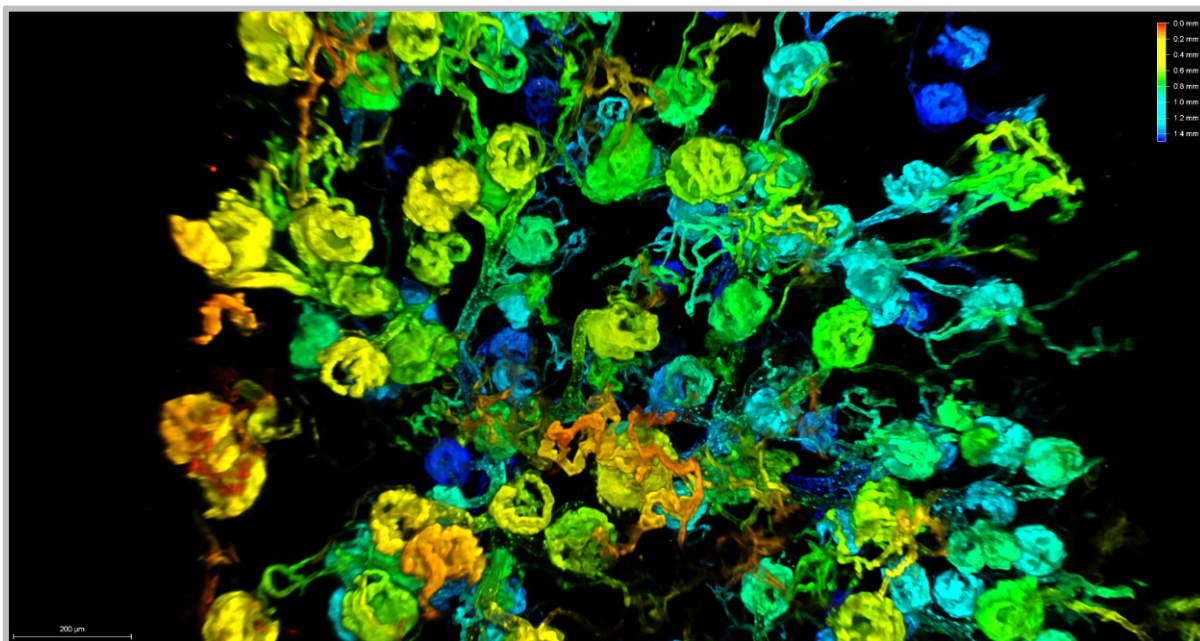
Figure 18 - Overview of a kidney section from a diabetic mouse. Altered perfusion pattern of the vascular tree and glomeruli when compared to wild-type kidneys. Color-coded image to improve depth perception from red (closer) to blue (farther).

Table 5 – Glomerular count and relation of valid, half-perfused or false negative glomeruli in standard optical subsets.

Group	Total count			Valid glomeruli (%)		Half-perfused (%)		False negative (%)	
	Mean	Min	Max	Min	Max	Min	Max	Min	Max
Wild-type	53	45	78	48	91	0	2	9	52
OB control	39	26	48	28	79	8	73	21	73
OB treatment	38	18	48	32	85	0	66	15	68

Wild-type subsets had an overall higher number of valid glomeruli and less percentage of false negative compared to diabetic mice. In contrast, diabetic mice had a distinct number of misperfused glomeruli that were almost inexistent in wild-type mice. Further qualitative analysis of our data allowed us to identify three different patterns of misperfused glomeruli: non-perfused, half-perfused, and center non-perfused glomeruli (Figure 19). All these patterns were observed in all diabetic mice and were almost absent in wild-type mice.
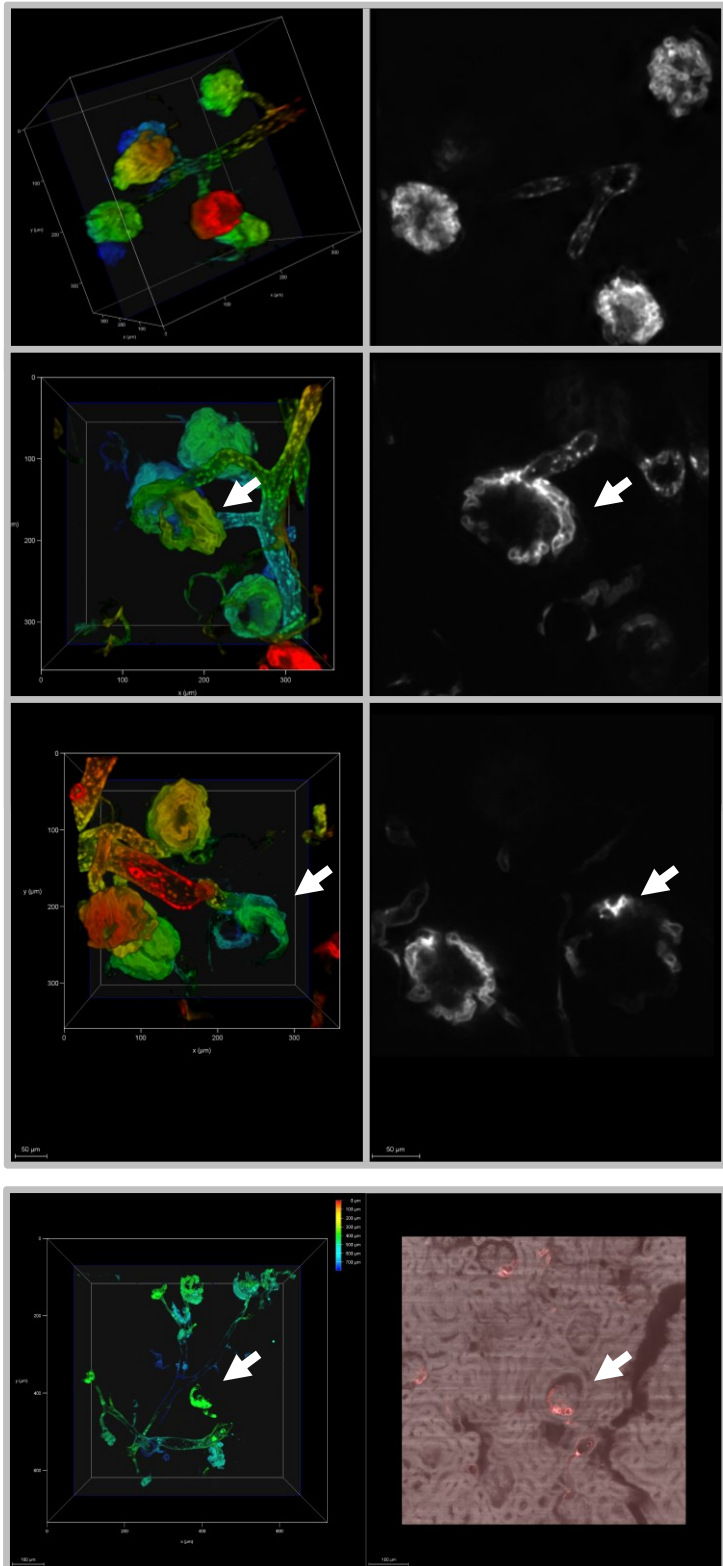
Figure 19 – Classes of glomeruli perfusion pattern. Three-dimensional (left) and optical section (right) aspect of perfused glomeruli. Color-coded image to improve depth perception from red (closer) to blue (farther). Gray color in right pictures represent MHI148-PEI perfusion. Arrows point out the class represented.

To substantiate the three-dimensional feature of misperfusion, we thin sliced non-cleared portions of the same kidneys used for clearing (Figure 20). Confocal images showed an uneven distribution of the dye in the capillary tuft of several glomeruli compared to wild-type mice. The same slices were stained for PAS subsequently. Comparison of slices before and after PAS staining showed that MHI148-PEI fluorescence was lost during the staining procedure. Nonetheless, it was possible to identify the same structures in both images. Areas surrounding non-perfused regions by MHI148-PEI presented intense ECM deposition in the mesangial area and/or glomerulosclerotic lesions (partial or total).
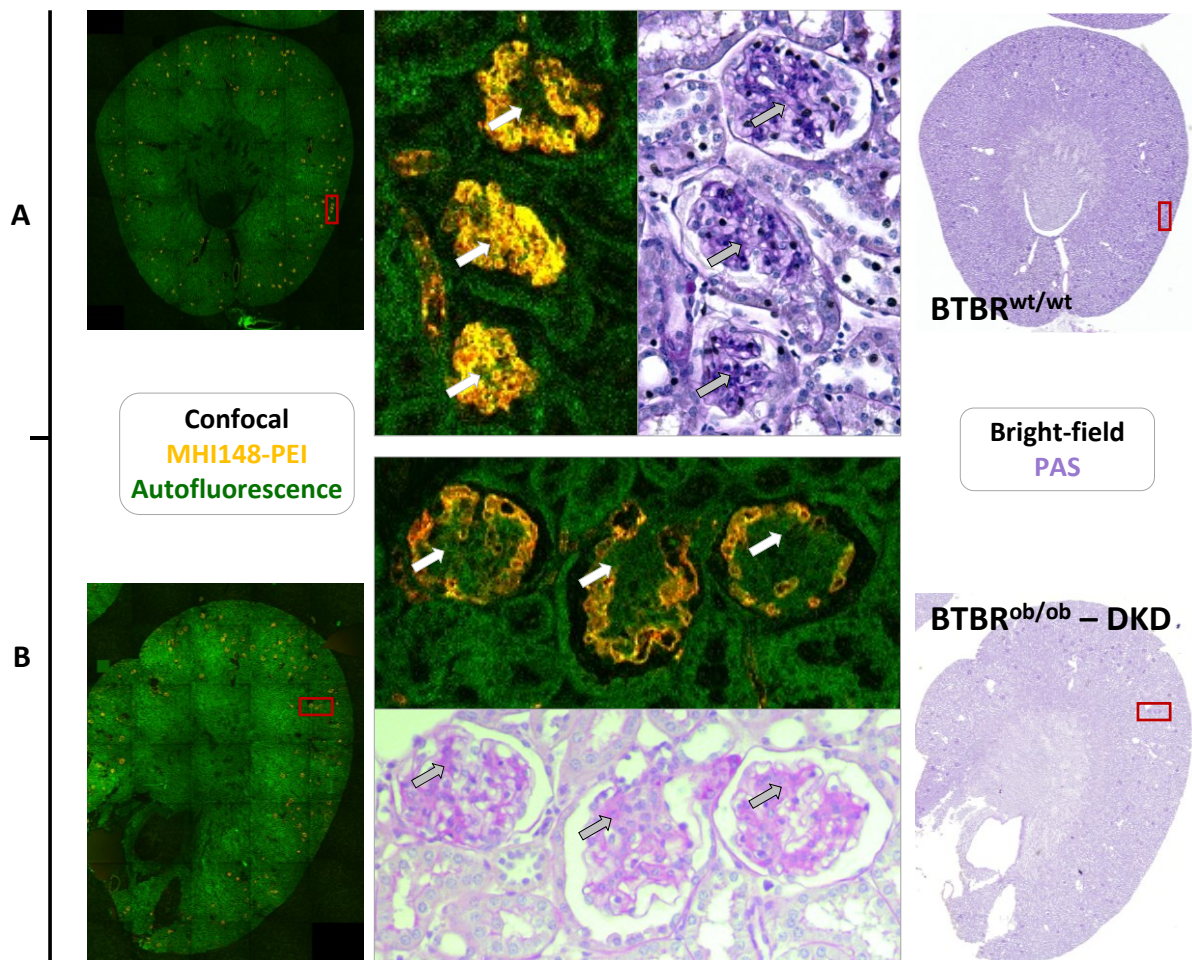

Figure 20 – Mesangial expansion in diabetic mice. Representative images of kidney sections imaged by confocal (left) and bright field (right) microscopy. Wild-type mice (A) present even distribution of MHI148-PEI in the glomerular tuft (orange staining) as compared to diabetic mice (B). Intense PAS positive regions in the mesangium of diabetic mice correlate with non-perfused areas by MHI148-PEI.

4. Discussion

The use of MSC as a potential therapy for DKD in a type-2 diabetic model was examined in the present work. In order to do so, two independent cohorts of BTBR$^{ob/ob}$ were treated with either human MSC isolated from adipose tissue or human MSC derived from dermis (cohorts hADSC and hABCB5+, respectively). Improvement of DKD was postulated as significant amelioration of any of the pathophysiological or histological known traits of DKD, or reported in type-1 or type-2 models treated with MSC (Table 1). This work also implemented new available methods, i.e. transcutaneous GFR and a tissue clearing methodology, to increase our understanding on functional and morphological changes in this model and better evaluate therapeutic efficacy.

Despite the large number of parameters evaluated, we did not observe a clear improvement on the course of DKD in mice treated with MSC. This was irrespective of the type of MSC used for intervention (hADSC or hABCB5+). The concise renal targets evaluated in this work were albumin excretion in urine, GFR, and glomerular changes: glomerular size, afferent dilation, and ECM deposition. Treatment with MSC did not affect the endpoints-free survival of diabetic mice in the study (Figure 5) nor hyperglycemia (Figure 7). Overall, mice from cohort hADSC had significantly less incidences regarding natural deaths or worsening condition compared to cohort hABCB5+. Additionally, glycated hemoglobin levels were categorically lower in cohort hADSC during the whole duration of the study so as fasting plasma glucose values (data not shown). The worse hyperglycemic condition of mice in cohort hABCB5+ might explain their early deterioration. Yet, differences in DKD features, such as marked differences in ECM deposition or albuminuria changes, were not observed when comparing cohorts. Treatment associated death was not considered to occur since death did not happen upon treatment but rather several weeks thereafter. Moreover, mortality was even higher in the untreated OB control group of the hABCB5+ cohort (Figure 5). An acute complication of diabetes (such as ketoacidosis) could be considered to explain this incidence in natural deaths, since most of the mice did not show signs of deterioration following the health assessment criteria (Table 2). It is worth mentioning that because of discontinuation in the production of cartridges used for HbA1c assessment, glycated hemoglobin was determined with a

different device in both cohorts. This might have contributed to the differences observed in glycation levels of both cohorts. Interestingly, most of the studies reviewed for this work showed significant reduction of hyperglycemia after MSC administration, which could contribute to remission in DKD progression. It has been suggested that STZ-induced models (such as in rats and C57BL/6 mice) are less susceptible to diabetes-associated kidney damage [34], which might contribute to the protective role of MSC reported in these models. Regarding mice that were euthanized, severe macroscopic lesions related to tumor growth were evident in areas of the abdominal cavity, so as single kidney macroplasia (Figure 6). MSC were discarded as possible cause of these lesions since they were present in at least 20% of the mice without a clear association to treatment or cohort and age. A final difference between both cohorts is the infection of ca. 80% of mice in cohort hADSC with mouse parvovirus during experimentation. Although it is unlikely that the parvovirus infection would affect renal targets, it cannot be excluded that this might have affected the efficiency of hADSC treatment.

Further parameters such as albuminuria and GFR were not improved by treatment. Albuminuria did not significantly differ at any time-point between groups after intervention. Still, a sustained trend for less albuminuria could be observed in OB treated mice compared to OB control (Figure 8) of both cohorts. This trend was particularly stable in cohort hADSC before its rapid return to OB control levels at week 23. Parameters of glomerular function such as renal clearance (which has not been recurrently studied to evaluate amelioration by MSC therapy) were almost identical at 24 weeks of age in cohort hADSC (Figure 9). Similarly, diabetic mice from cohort hABCB5+ did not differ in renal clearance at earlier time-points of 17 and 21 weeks of age, neither in comparison to wild-type values at 21 weeks. Estimated GFR normalized by weight (as shown in Table 4) did not show differences as well. Still, a joint comparison of values in Table 4 suggests that diabetic mice might develop hyperfiltration with age, as at 24 weeks the GFR of cohort hADSC doubles the values in wild-type mice at 17 weeks, and is higher than in younger diabetic mice of cohort hABCB5+. An argument in favor of this result is that GFR in healthy rodents is expected to decrease with age as it has been shown by a different GFR estimation method [40]. Still, age-matched wild type GFR measurements are required to confirm this data.

One of the most reported improvements by MSC intervention in diabetic animal models is the reduction of ECM deposition in the mesangial area (i.e. mesangial expansion) and reduced glomerular enlargement compared to age-matched diabetic mice [58]. In our study, glomerular lesions were identified in PAS-stained slices such as glomerular enlargement, diffuse mesangial expansion, and different degrees of glomerulosclerosis in contrast to wild-type kidney sections. The observed histological parameters were similar in non-treated diabetic mice compared to treatment, implying that MSC were not able to reduce the course of DKD at histological level. A critical evaluation on the studies reviewed in Table 1 shows that different levels of information were used to assess the benefit of MSC at histological level. First, most of the histopathological approaches employed focused on qualitative information of remission of glomerular lesions without scoring or were unable to find improvement [61, 65, 67-69, 74, 75, 80, 82, 83]. This has been settled in other studies by scoring in blinded experiments [66, 70, 79], semi-quantitative statements based on the averaged percentages of incidence of glomerular lesions [62-64, 78, 81] and antibody staining of ECM upregulated proteins produced in DKD, or podocyte damage [71-73, 76, 77]. However, the level of information about a whole glomerulus is restricted to cross-sectional examination, which might be prone to the introduction of bias by unexperienced researchers. In order to improve the quality of our data towards quantitative analysis, further histological comparisons such as enlargement of the glomeruli, afferent arteriole dilation and their correlation were conducted with the implementation of tissue clearing and perfusion staining.

Tissue clearing in combination with dark-field microscopy and perfusion staining are a novel set of techniques recently described for the study of the kidney [94]. The protocol implemented in this research work has been previously described and developed by Huang et al. (2019) for healthy mice [90]. A center portion of the work conducted here was the successful implementation of this method, from tissue preparation to tissue analysis as a complementary morphometric analysis on the kidney of the BTBR[ob/ob] model (Figure 11). This fast methodology of tissue clearing granted the ability to evaluate histological features in a robust three-dimensional, semi-quantitative and reproducible way that complements to what it is known from DKD features. Previous publications from our group have reported an overall increase of glomerular size in diabetic mice using classical histology and PAS

staining [37, 93]. These findings have been consistently observed in our data with a tissue clearing approach on thick portions of kidneys from diabetic mice with respect to wild type mice (Figure 11, C). We have conceived a semi-automatic workflow to measure glomerular enlargement with an unbiased three-dimensional morphometric method of a large representative number of glomeruli contained in standard optical sections. More importantly, the portion of kidney analyzed is a representative sample of the full organ, as we have observed similar size distributions in pole, center and mid-center areas of the same kidney (Figure 12). Nonetheless, our method of analysis is not exempt of errors. Validation of the identified glomeruli for analysis showed a systematic error up to 20% false negative glomeruli (valid glomeruli, but not identified by the pipeline). Still, this is an acceptable error for our purpose since an average of 30 glomeruli per section is expected to be included in the analysis, and the overlapping between wild-type and diabetic size distributions is sufficiently low (Figure 11, C). Thus, the number of glomeruli that are correctly classified is still representative of the size distribution of the original kidney. Being systematic, this 20% error will be subject to improvement by modifying aspects in our pipeline with customized approaches of segmentation like increasing the input data for training the deep-learning algorithms.

The approach used in this work for three-dimensional analysis makes use of perfusion of MHI148-PEI as staining method to study microvascular lesions. Unlike antibody staining, MHI148-PEI can be considered an unspecific dye due to its chemical tagging through ionic affinity. This aspect increases the efficiency of the methodology as it stains vessels in a homogeneous way, but relies on correct perfusion and chemical stability of the areas to be stained. Early results obtained with this methodology led us to consider problems in protocol implementation as kidneys from diabetic mice were in many cases not properly perfused in glomerular areas (Figure 17 & Figure 18). A thorough examination of perfusion patterns including wild-type kidneys demonstrated that these were exclusively characteristic of diabetic animals, as in the standard optical subsets employed for morphometry, only one glomerulus presented abnormal perfusion (Table 5). It is worth to mention that vessel structures exist (visible by autofluorescence evaluation), discarding the alternative explanation of atrophic glomeruli.

Three types of misperfused glomeruli could be identified in our data: non-perfused, half-perfused and central non-perfused (Figure 19). Non-perfused glomeruli do not present MHI148-PEI fluorescence in tuft structures and their three-dimensional aspect is similar to "buds" in a vascular branch. This first category can be found in wild-type mice, but very rarely. Half-perfused glomeruli have been exclusively seen in diabetic mice, where their three-dimensional aspect shows only the half portion of the tuft connected to their afference. Finally, center non-perfused glomeruli have been observed in wild-type mice with very low frequency, while in diabetic mice they can be present in a ratio of 3:1 to completely perfused glomeruli (depending on extension of DKD lesions). The three-dimensional aspect of the latter is variable, ranging from apparent fully perfused glomeruli with a hollow center to an empty semi-ellipsoid. However, in all cases afferent and presumably the efferent arteriole are visible.

Following these observations, we hypothesize that these patterns were caused by mesangial expansion (center non-perfused) and partial glomerulosclerotic (half non-perfused) DKD lesions. Examination of kidney sections perfused with MHI148-PEI before and after PAS staining showed that glomeruli with some degree of glomerulosclerosis were partially not stained (data not shown), and glomeruli with areas where there was no MHI148-PEI staining were in fact areas with increased ECM deposition in the mesangial area (Figure 20). As a result, peripheral vessels of the tuft without glomerulosclerosis are evenly stained while the ones in the mesangial area are not. An explanation to this observation might be that when perfusion reaches the glomeruli, the flow follows the path of least resistance, which in this case corresponds to the outer vessels of the tuft. An alternative explanation might be the loss of negative charge in the endothelium due to hyperglycemia. It is widely accepted that hyperglycemia induces glycocalix changes in endothelium cells, which might have reduced the efficiency of MHI148-PEI staining due to loss in negative charge. However, this would not explain why only the center of the glomerulus lacks staining, while afferent and efferent arterioles, and post-tubular capillaries of the same glomerulus are also stained. Taken this information together, this methodology may reflect the three-dimensional aspect of DKD lesions through the perfusion pattern of MHI148-PEI; that is, half-perfused glomeruli represent partial glomerulosclerotic lesions, and center non-perfused glomeruli represent expansion of the mesangium. Finally, we do not consider dye leakage through the glomerular

filtration barrier as explanation, since MHI148-PEI signal in Bowman's capsule or tubules was negligible.

The analysis of structures in a three-dimensional way was conducted in cohort hABCB5+ since the methodology was implemented after the experimentation with cohort hADSC. Three-dimensional analysis of the impact of MSC in histology of the BTBR$^{ob/ob}$ did not show differences. Two main features were estimated from standard optical subsets of 1mm^3: Feret's diameter, and the diameter of the afferent arteriole as a sign of hyperfiltration. Statistical differences were only found between wild-type mice and the OB treated group, while almost significant against OB control for Feret's diameter (*p-value* = 0.0599) (Figure 13). We presume that this observation may be due to the small group size of OB control compared to OB treated (n = 3 vs. n = 6). Following the tubular hypothesis of hyperfiltration in diabetes [95], dilation of the afferent arteriole may indicate a failure in the tubuloglomerular feedback due to hyperglycemia, together with a constriction of the efferent arteriole. Indeed, diabetic mice irrespective of treatment showed a significant dilation of the afferent arteriole when compared to wild-type mice (Figure 14). Visible efferent arterioles of fewer glomeruli may confirm this observation since in diabetic mice the efferent arterioles are much more constricted in contrast to wild-type mice (Figure 15). However, this observation could not be formally quantified by our approach due to low signal-to background fluorescence ratio. A bivariate linear regression analysis between the above-mentioned variables (that is, the correlation between afferent arteriole's diameter and the corresponding Feret's diameter of the same glomerulus) showed a positive correlation in the overall dataset (Figure 16). Interestingly, OB control mice, but not wild type, followed this trend. This supports that hyperfiltration might be occurring as consequence of tubuloglomerular feedback's disruption due to reduced sodium reabsorption in the distal tubule. Yet, this last statement would need to be confirmed by incorporating the diameter of the efferent arteriole into the analysis, and perhaps an additional diabetic group treated with SGLT-2 inhibitors.

Taken these results together, OB treated mice in both cohorts did not show signs of improvement at histological or pathophysiological level as it has been reported in alternative DKD models. Our histology results clearly showed no improvement in DKD course as glomerular size, dilation of afferent arteriole, and ECM deposition did

not differ from non-treated diabetics. GFR also did not show signs of improvement, at least at the end of the experiment. Even though albuminuria results did not present differences at statistical level, the observed trend to lower albumin excretion in treated mice might imply a plausible transient effect of MSC. This could be confirmed by increasing the initial administration dosage, or performing a second intervention between 15-19 weeks of age. Alternatively, an earlier intervention as a protective (rather an ameliorating) role of MSC might show a positive course of DKD in this model. Future studies would need to consider this information to elucidate the possible benefit of MSC in type-2 DKD mice models such as the BTBR presented here.

5. Summary

The use of mesenchymal stromal cells (MSC) in diabetic models as a possible therapy to ameliorate diabetic kidney disease (DKD) is not new. Several researchers have conducted successful experiments reporting improvement on the course of DKD after MSC interventions. However, most of the research focuses on type-1 diabetes, particularly using Streptozotocin-induced rodents as model. In order to demonstrate the true potential of MSC as a therapeutic option for DKD, further studies must also expand the research on alternative diabetic models. In this study, we have evaluated the impact of two different human MSC on the BTBR[ob/ob] mice model (a type-2 diabetes model, susceptible to hyperglycemia-associated kidney damage) that closely resembles the pathogenesis in humans.

Adipose-derived (hADSC) or dermis-derived (hABCB5+) MSC were administered intravenously to two independent cohorts of 12 weeks-old BTBR[ob/ob] mice and followed-up until 24-26 weeks of age. Key parameters in which MSC showed amelioration by previous studies were observed, such as albuminuria and histology of glomerular lesions. Additionally, two new methodological approaches were implemented to better evaluate therapeutic efficacy and increase our understanding of functional and morphological changes in the BTBR: transcutaneous glomerular filtration rate and a semi-quantitative methodology based on tissue clearing and three-dimensional analysis.

Weak evidence of improvement by MSC on DKD was found at functional level by lowering albumin excretion in urine of diabetic treated groups in both cohorts. Although the observed changes were not significant, two independent experiments showed similar trends to what is reported in the literature. Still, this tendency was not transduced in improvement of conventional histology or transcutaneous measurements of glomerular filtration rate after its implementation.

Although the benefit of MSC could not be proven in this model, important findings were made after the successful implementation of the above-mentioned tissue clearing approach in terms of robust morphometrical analysis (glomerular size and afferent arteriole dilation), and glomerular perfusion patterns in DKD that seem to go along with mesangial proliferation and glomerulosclerosis.

6. References

1.   American Diabetes, A., *2. Classification and Diagnosis of Diabetes: Standards of Medical Care in Diabetes-2020.* Diabetes Care, 2020. **43**(Suppl 1): p. S14-S31.

2.   Saeedi, P., et al., *Global and regional diabetes prevalence estimates for 2019 and projections for 2030 and 2045: Results from the International Diabetes Federation Diabetes Atlas, 9(th) edition.* Diabetes Res Clin Pract, 2019. **157**: p. 107843.

3.   International Expert, C., *International Expert Committee report on the role of the A1C assay in the diagnosis of diabetes.* Diabetes Care, 2009. **32**(7): p. 1327-34.

4.   Umpierrez, G. and M. Korytkowski, *Diabetic emergencies - ketoacidosis, hyperglycaemic hyperosmolar state and hypoglycaemia.* Nat Rev Endocrinol, 2016. **12**(4): p. 222-32.

5.   Forbes, J.M. and M.E. Cooper, *Mechanisms of diabetic complications.* Physiol Rev, 2013. **93**(1): p. 137-88.

6.   *2016 USRDS annual data report: epidemiology of kidney disease in the United States*. 2016, National Institutes of Health, National Institute of Diabetes and Digestive and Kidney Diseases, Bethesda, MD: United States Renal Data System.

7.   Fioretto, P. and M. Mauer, *Histopathology of diabetic nephropathy.* Seminars in nephrology, 2007. **27**(2): p. 195-207.

8.   Ponchiardi, C., M. Mauer, and B. Najafian, *Temporal profile of diabetic nephropathy pathologic changes.* Curr Diab Rep, 2013. **13**(4): p. 592-9.

9.   Thomas, M.C., et al., *Diabetic kidney disease.* Nat Rev Dis Primers, 2015. **1**: p. 15018.

10.   Schalkwijk, C.G. and C.D.A. Stehouwer, *Methylglyoxal, a Highly Reactive Dicarbonyl Compound, in Diabetes, Its Vascular Complications, and Other Age-Related Diseases.* Physiol Rev, 2020. **100**(1): p. 407-461.

11.   Brownlee, M., *The Pathobiology of Diabetic Complications.* Diabetes, 2005. **54**(6): p. 1615.

12.   Kaiser, N., et al., *Differential Regulation of Glucose Transport and Transporters by Glucose in Vascular Endothelial and Smooth Muscle Cells.* Diabetes, 1993. **42**(1): p. 80.

13.   Heilig, C.W., et al., *Overexpression of glucose transporters in rat mesangial cells cultured in a normal glucose milieu mimics the diabetic phenotype.* The Journal of Clinical Investigation, 1995. **96**(4): p. 1802-1814.

14.   Li, J.J., et al., *Podocyte biology in diabetic nephropathy.* Kidney Int Suppl, 2007(106): p. S36-42.

15.   Mora-Fernandez, C., et al., *Diabetic kidney disease: from physiology to therapeutics.* J Physiol, 2014. **592**(18): p. 3997-4012.

16.   Marshall, C.B., *Rethinking glomerular basement membrane thickening in diabetic nephropathy: adaptive or pathogenic?* Am J Physiol Renal Physiol, 2016. **311**(5): p. F831-F843.

17.   Mason, R.M. and N.A. Wahab, *Extracellular matrix metabolism in diabetic nephropathy.* J Am Soc Nephrol, 2003. **14**(5): p. 1358-73.

18.   Brenner, B.M., E.V. Lawler, and H.S. Mackenzie, *The hyperfiltration theory: a paradigm shift in nephrology.* Kidney Int, 1996. **49**(6): p. 1774-7.

19.   Kriz, W., et al., *The podocyte's response to stress: the enigma of foot process effacement.* Am J Physiol Renal Physiol, 2013. **304**(4): p. F333-47.

20.   Lin, J.S. and K. Susztak, *Podocytes: the Weakest Link in Diabetic Kidney Disease?* Curr Diab Rep, 2016. **16**(5): p. 45.

21.   Cravedi, P., P. Ruggenenti, and G. Remuzzi, *Proteinuria should be used as a surrogate in CKD.* Nat Rev Nephrol, 2012. **8**(5): p. 301-6.

22.   Jefferson, J.A., S.J. Shankland, and R.H. Pichler, *Proteinuria in diabetic kidney disease: a mechanistic viewpoint.* Kidney Int, 2008. **74**(1): p. 22-36.

23.   Suh, J.H. and J.H. Miner, *The glomerular basement membrane as a barrier to albumin.* Nat Rev Nephrol, 2013. **9**(8): p. 470-7.

24.   Haraldsson, B. and M. Jeansson, *Glomerular filtration barrier.* Curr Opin Nephrol Hypertens, 2009. **18**(4): p. 331-5.

25.   Abbate, M., C. Zoja, and G. Remuzzi, *How does proteinuria cause progressive renal damage?* J Am Soc Nephrol, 2006. **17**(11): p. 2974-84.

26.   Flyvbjerg, A., *The role of the complement system in diabetic nephropathy.* Nature Reviews Nephrology, 2017. **13**(5): p. 311-318.

27.   Carlstrom, M., C.S. Wilcox, and W.J. Arendshorst, *Renal autoregulation in health and disease.* Physiol Rev, 2015. **95**(2): p. 405-511.

28.   Helal, I., et al., *Glomerular hyperfiltration: definitions, mechanisms and clinical implications.* Nat Rev Nephrol, 2012. **8**(5): p. 293-300.

29.   Tonneijck, L., et al., *Glomerular Hyperfiltration in Diabetes: Mechanisms, Clinical Significance, and Treatment.* J Am Soc Nephrol, 2017. **28**(4): p. 1023-1039.

30.   De Nicola, L., G. Conte, and R. Minutolo, *Prediabetes as a Precursor to Diabetic Kidney Disease.* Am J Kidney Dis, 2016. **67**(6): p. 817-9.

31.   Melsom, T., et al., *Prediabetes and Risk of Glomerular Hyperfiltration and Albuminuria in the General Nondiabetic Population: A Prospective Cohort Study.* Am J Kidney Dis, 2016. **67**(6): p. 841-50.

32.   Gaspari, F., et al., *The GFR and GFR decline cannot be accurately estimated in type 2 diabetics.* Kidney Int, 2013. **84**(1): p. 164-73.

33.   Chen, C., et al., *Normoalbuminuric diabetic kidney disease.* Front Med, 2017. **11**(3): p. 310-318.

34.   Kitada, M., Y. Ogura, and D. Koya, *Rodent models of diabetic nephropathy: their utility and limitations.* Int J Nephrol Renovasc Dis, 2016. **9**: p. 279-290.

35.   Betz, B. and B.R. Conway, *An Update on the Use of Animal Models in Diabetic Nephropathy Research.* Curr Diab Rep, 2016. **16**(2): p. 18.

36.   Nakayama, T., et al., *Endothelial injury due to eNOS deficiency accelerates the progression of chronic renal disease in the mouse.* Am J Physiol Renal Physiol, 2009. **296**(2): p. F317-27.

37.   Qiu, J., et al., *Human carnosinase 1 overexpression aggravates diabetes and renal impairment in BTBR(Ob/Ob) mice.* J Mol Med (Berl), 2020.

38.   Eisner, C., et al., *Major contribution of tubular secretion to creatinine clearance in mice.* Kidney Int, 2010. **77**(6): p. 519-26.

39.   Qi, Z., et al., *Serial determination of glomerular filtration rate in conscious mice using FITC-inulin clearance.* American Journal of Physiology-Renal Physiology, 2004. **286**(3): p. F590-F596.

40.   Sasaki, Y., et al., *Estimation of glomerular filtration rate in conscious mice using a simplified equation.* Physiol Rep, 2014. **2**(8).

41.   Pill, J., et al., *Fluorescein-labeled sinistrin as marker of glomerular filtration rate.* Eur J Med Chem, 2005. **40**(10): p. 1056-61.

42.   Schreiber, A., et al., *Transcutaneous measurement of renal function in conscious mice.* Am J Physiol Renal Physiol, 2012. **303**(5): p. F783-8.

43.   McManus, J.F.A., *The periodic acid routing applied to the kidney.* The American journal of pathology, 1948. **24**(3): p. 643-653.

44.   Sheehan, S.M. and R. Korstanje, *Automatic glomerular identification and quantification of histological phenotypes using image analysis and machine learning.* Am J Physiol Renal Physiol, 2018. **315**(6): p. F1644-F1651.

45.   Richardson, D.S. and J.W. Lichtman, *Clarifying Tissue Clearing.* Cell, 2015. **162**(2): p. 246-257.

46.   Elfer, K.N., et al., *DRAQ5 and Eosin ('D&E') as an Analog to Hematoxylin and Eosin for Rapid Fluorescence Histology of Fresh Tissues.* PLoS One, 2016. **11**(10): p. e0165530.

47.   Zhang, Y., et al., *Spectral Characteristics of Autofluorescence in Renal Tissue and Methods for Reducing Fluorescence Background in Confocal Laser Scanning Microscopy.* J Fluoresc, 2018. **28**(2): p. 561-572.

48.   Neumiller, J.J., R.Z. Alicic, and K.R. Tuttle, *Therapeutic Considerations for Antihyperglycemic Agents in Diabetic Kidney Disease.* J Am Soc Nephrol, 2017. **28**(8): p. 2263-2274.

49.   Bergenstal, R.M., C.J. Bailey, and D.M. Kendall, *Type 2 diabetes: assessing the relative risks and benefits of glucose-lowering medications.* Am J Med, 2010. **123**(4): p. 374 e 9 -18.

50.   Fioretto, P., et al., *SGLT2 Inhibitors and the Diabetic Kidney.* Diabetes Care, 2016. **39 Suppl 2**: p. S165-71.

51.   Lupsa, B.C. and S.E. Inzucchi, *Use of SGLT2 inhibitors in type 2 diabetes: weighing the risks and benefits.* Diabetologia, 2018. **61**(10): p. 2118-2125.

52.   Palmer, S.C., et al., *Comparative efficacy and safety of blood pressure-lowering agents in adults with diabetes and kidney disease: a network meta-analysis.* The Lancet, 2015. **385**(9982): p. 2047-2056.

53.   Ptinopoulou, A.G., M.I. Pikilidou, and A.N. Lasaridis, *The effect of antihypertensive drugs on chronic kidney disease: a comprehensive review.* Hypertens Res, 2013. **36**(2): p. 91-101.

54.   Remuzzi, G., A. Benigni, and A. Remuzzi, *Mechanisms of progression and regression of renal lesions of chronic nephropathies and diabetes.* J Clin Invest, 2006. **116**(2): p. 288-96.

55.   Romagnani, P. and G. Remuzzi, *Renal progenitors in non-diabetic and diabetic nephropathies.* Trends Endocrinol Metab, 2013. **24**(1): p. 13-20.

56.   Appel, D., et al., *Recruitment of podocytes from glomerular parietal epithelial cells.* J Am Soc Nephrol, 2009. **20**(2): p. 333-43.

57.   Ronconi, E., et al., *Regeneration of glomerular podocytes by human renal progenitors.* J Am Soc Nephrol, 2009. **20**(2): p. 322-32.

58.   Torres Crigna, A., et al., *Stem/Stromal Cells for Treatment of Kidney Injuries With Focus on Preclinical Models.* Front Med (Lausanne), 2018. **5**: p. 179.

59.   Benigni, A., M. Morigi, and G. Remuzzi, *Kidney regeneration.* Lancet, 2010. **375**: p. 1310-7.

60.   Chen, J., et al., *Adoptive transfer of syngeneic bone marrow-derived cells in mice with obesity-induced diabetes: selenoorganic antioxidant ebselen restores stem cell competence.* Am J Pathol, 2009. **174**(2): p. 701-11.

61. Lee, R.H., et al., *Multipotent stromal cells from human marrow home to and promote repair of pancreatic islets and renal glomeruli in diabetic NOD/scid mice.* Proc Natl Acad Sci U S A, 2006. **103**(46): p. 17438-43.

62. Park, J.H., et al., *Human umbilical cord blood-derived mesenchymal stem cells prevent diabetic renal injury through paracrine action.* Diabetes Res Clin Pract, 2012. **98**(3): p. 465-73.

63. Ezquer, F., et al., *Proregenerative Microenvironment Triggered by Donor Mesenchymal Stem Cells Preserves Renal Function and Structure in Mice with Severe Diabetes Mellitus.* Biomed Res Int, 2015. **2015**: p. 164703.

64. Nagaishi, K., et al., *Mesenchymal stem cell therapy ameliorates diabetic nephropathy via the paracrine effect of renal trophic factors including exosomes.* Sci Rep, 2016. **6**: p. 34842.

65. Ezquer, F.E., et al., *Systemic administration of multipotent mesenchymal stromal cells reverts hyperglycemia and prevents nephropathy in type 1 diabetic mice.* Biol Blood Marrow Transplant, 2008. **14**(6): p. 631-40.

66. Ezquer, F., et al., *Endovenous administration of bone-marrow-derived multipotent mesenchymal stromal cells prevents renal failure in diabetic mice.* Biol Blood Marrow Transplant, 2009. **15**(11): p. 1354-65.

67. Zhou, H., et al., *Mesenchymal stem cells transplantation mildly ameliorates experimental diabetic nephropathy in rats.* Chin Med J (Engl), 2009. **122**(21): p. 2573-9.

68. Ouyang, J.Y., et al., *Preventive effects of syngeneic bone marrow transplantation on diabetic nephropathy in mice.* Transplant Immunology, 2010. **22**(3-4): p. 184-190.

69. Fang, Y., et al., *Autologous transplantation of adipose-derived mesenchymal stem cells ameliorates streptozotocin-induced diabetic nephropathy in rats by inhibiting oxidative stress, pro-inflammatory cytokines and the p38 MAPK signaling pathway.* Int J Mol Med, 2012. **30**(1): p. 85-92.

70. Masoad, R.E., et al., *Effect of mononuclear cells versus pioglitazone on streptozotocin-induced diabetic nephropathy in rats.* Pharmacol Rep, 2012. **64**(5): p. 1223-33.

71. Lv, S.S., et al., *Mesenchymal stem cells transplantation ameliorates glomerular injury in streptozotocin-induced diabetic nephropathy in rats via inhibiting macrophage infiltration.* Int Immunopharmacol, 2013. **17**(2): p. 275-82.

72. Wang, S., et al., *Mesenchymal stem cells ameliorate podocyte injury and proteinuria in a type 1 diabetic nephropathy rat model.* Biol Blood Marrow Transplant, 2013. **19**(4): p. 538-46.

73. Zhang, L., et al., *Repeated systemic administration of human adipose-derived stem cells attenuates overt diabetic nephropathy in rats.* Stem Cells Dev, 2013. **22**(23): p. 3074-86.

74. Zhang, Y., et al., *Kidney-targeted transplantation of mesenchymal stem cells by ultrasound-targeted microbubble destruction promotes kidney repair in diabetic nephropathy rats.* Biomed Res Int, 2013. **2013**: p. 526367.

75. Abdel Aziz, M.T., et al., *The role of bone marrow derived-mesenchymal stem cells in attenuation of kidney function in rats with diabetic nephropathy.* Diabetol Metab Syndr, 2014. **6**(1): p. 34.

76. Lv, S., et al., *Mesenchymal stem cells transplantation ameliorates glomerular injury in streptozotocin-induced diabetic nephropathy in rats via inhibiting oxidative stress.* Diabetes Res Clin Pract, 2014. **104**(1): p. 143-54.

77. Lv, S., et al., *Mesenchymal stem cells ameliorate diabetic glomerular fibrosis in vivo and in vitro by inhibiting TGF-beta signalling via secretion of bone morphogenetic protein 7.* Diab Vasc Dis Res, 2014. **11**(4): p. 251-261.

78. Pan, X.H., et al., *Bone-marrow mesenchymal stem cell transplantation to treat diabetic nephropathy in tree shrews.* Cell Biochem Funct, 2014. **32**(5): p. 453-63.

79. Ni, W., et al., *Adipose-Derived Mesenchymal Stem Cells Transplantation Alleviates Renal Injury in Streptozotocin-Induced Diabetic Nephropathy.* J Histochem Cytochem, 2015. **63**(11): p. 842-53.

80. Hamza, A.H., et al., *Mesenchymal stem cells: a future experimental exploration for recession of diabetic nephropathy.* Ren Fail, 2016. **39**(1): p. 67-76.

81. Jiang, Z.Z., et al., *Exosomes secreted by human urine-derived stem cells could prevent kidney complications from type I diabetes in rats.* Stem Cell Res Ther, 2016. **7**: p. 24.

82. Lang, H. and C. Dai, *Effects of Bone Marrow Mesenchymal Stem Cells on Plasminogen Activator Inhibitor-1 and Renal Fibrosis in Rats with Diabetic Nephropathy.* Arch Med Res, 2016. **47**(2): p. 71-7.

83. Nagaishi, K., et al., *Umbilical cord extracts improve diabetic abnormalities in bone marrow-derived mesenchymal stem cells and increase their therapeutic effects on diabetic nephropathy.* Sci Rep, 2017. **7**(1): p. 8484.

84. Hudkins, K.L., et al., *BTBR Ob/Ob mutant mice model progressive diabetic nephropathy.* J Am Soc Nephrol, 2010. **21**(9): p. 1533-42.

85. Zuk, P.A., et al., *Human adipose tissue is a source of multipotent stem cells.* Mol Biol Cell, 2002. **13**(12): p. 4279-95.

86. Kern, S., et al., *Comparative analysis of mesenchymal stem cells from bone marrow, umbilical cord blood, or adipose tissue.* Stem Cells, 2006. **24**(5): p. 1294-301.

87. Kocaoemer, A., et al., *Human AB serum and thrombin-activated platelet-rich plasma are suitable alternatives to fetal calf serum for the expansion of mesenchymal stem cells from adipose tissue.* Stem Cells, 2007. **25**(5): p. 1270-8.

88. Tappenbeck, N., et al., *In vivo safety profile and biodistribution of GMP-manufactured human skin-derived ABCB5-positive mesenchymal stromal cells for use in clinical trials.* Cytotherapy, 2019. **21**(5): p. 546-560.

89. Herrera Pérez, Z., S. Weinfurter, and N. Gretz, *Transcutaneous Assessment of Renal Function in Conscious Rodents.* JoVE, 2016(109): p. e53767.

90. Huang, J., et al., *A cationic near infrared fluorescent agent and ethyl-cinnamate tissue clearing protocol for vascular staining and imaging.* Sci Rep, 2019. **9**(1): p. 521.

91. Bolte, S. and F.P. CordeliÈRes, *A guided tour into subcellular colocalization analysis in light microscopy.* Journal of Microscopy, 2006. **224**(3): p. 213-232.

92. Ollion, J., et al., *TANGO: a generic tool for high-throughput 3D image analysis for studying nuclear organization.* Bioinformatics, 2013. **29**(14): p. 1840-1.

93. Albrecht, T., et al., *Carnosine Attenuates the Development of both Type 2 Diabetes and Diabetic Nephropathy in BTBR ob/ob Mice.* Sci Rep, 2017. **7**: p. 44492.

94. Klingberg, A., et al., *Fully Automated Evaluation of Total Glomerular Number and Capillary Tuft Size in Nephritic Kidneys Using Lightsheet Microscopy.* Journal of the American Society of Nephrology : JASN, 2017. **28**(2): p. 452-459.

95. Vallon, V. and S.C. Thomson, *The tubular hypothesis of nephron filtration and diabetic kidney disease.* Nat Rev Nephrol, 2020. **16**(6): p. 317-336.

7. Curriculum Vitae and Publications

PERSONAL INFORMATION

Name   Diego Orlando Pastene Maldonado

Date of Birth   05.10.1986

Place of birth   Santiago (Chile)

Nationality   Chilean

Civil status   Single

SCHOOLING

2000-2004   High School Diploma
                                      "Instituto Santa María"
                                      Santiago (Chile)

UNIVERSITY EDUCATION

June, 2016 – up to now   Ph.D. Student
                                      Fifth Medical Department (Nephrology, Endocrinology, Rheumatology) of Mannheim University Hospital
                                      University of Heidelberg (Germany)

September, 2014 - January, 2016   M.Sc. Analytical and Bioanalytical sciences
                                      Thesis title: *"Absolute Quantification of Angiotensin II by Isotope Dilution Mass Spectrometry"* (Spanish)
                                      Faculty of Chemistry
                                      University of Oviedo (Spain)

September, 2009 - July, 2014   B.Sc. Biology
                                      Faculty of Biology
                                      University of Oviedo (Spain)

RESEARCH ACTIVITY

Publications

1. Qiu, J., T. Albrecht, S. Zhang, S. J. Hauske, A. Rodriguez-Nino, X. Zhang, D. Nosan, **D. O. Pastene**, C. Sticht, C. Delatorre, H. van Goor, S. Porubsky, B. K. Kramer and B. A. Yard **(2020)**. *"Human carnosinase 1 overexpression aggravates diabetes and renal impairment in BTBR(Ob/Ob) mice."* J Mol Med (Berl). DOI: 10.1007/s00109-020-01957-0

2. Qiu, J., S. J. Hauske, S. Zhang, A. Rodriguez-Nino, T. Albrecht, **D. O. Pastene**, J. van den Born, H. van Goor, S. Ruf, M. Kohlmann, M. Teufel, B. K. Kramer, H. P. Hammes, V. Peters, B. A. Yard and A. Kannt **(2019)**. *"Identification and characterisation of carnostatine (SAN9812), a potent and selective carnosinase (CN1) inhibitor with in vivo activity."* Amino Acids 51(1): 7-16. DOI: 10.1007/s00726-018-2601-z

3. Braun, J. D., **D. O. Pastene**, A. Breedijk, A. Rodriguez, B. B. Hofmann, C. Sticht, E. von Ochsenstein, H. Allgayer, J. van den Born, S. Bakker, S. J. Hauske, B. K. Kramer, B. A. Yard and T. Albrecht **(2019)**. *"Methylglyoxal down-regulates the expression of cell cycle associated genes and activates the p53 pathway in human umbilical vein endothelial cells."* Sci Rep 9(1): 1152. DOI: 10.1038/s41598-018-37937-1

4. Torres Crigna, A., C. Daniele, C. Gamez, S. Medina Balbuena, **D. O. Pastene**, D. Nardozi, C. Brenna, B. Yard, N. Gretz and K. Bieback **(2018)**. *"Stem/Stromal Cells for Treatment of Kidney Injuries with Focus on Preclinical Models."* Front Med (Lausanne) 5: 179. DOI: 10.3389/fmed.2018.00179

5. Albrecht, T., M. Schilperoort, S. Zhang, J. D. Braun, J. Qiu, A. Rodriguez, **D. O. Pastene**, B. K. Kramer, H. Koppel, H. Baelde, E. de Heer, A. Anna Altomare, L. Regazzoni, A. Denisi, G. Aldini, J. van den Born, B. A. Yard and S. J. Hauske **(2017)**. *"Carnosine Attenuates the Development of both Type 2 Diabetes and Diabetic Nephropathy in BTBR ob/ob Mice."* Sci Rep 7: 44492. DOI: 10.1038/srep44492

Poster presentations

1. **D. O. Pastene**, S. Hettler, N. Gretz, B. A. Yard, B. K. Krämer. "*Tissue clearing in combination with MHI148-PEI perfusion reveals perfusion abnormalities in glomerular areas of mesangial matrix expansion in diabetic BTBR$^{ob/ob}$ mice*" – Presented at "12th Jahrestagung der Deutschen Gesellschaft für Nephrologie" in Berlin (October, 2020)

8. Acknowledgements

Finally, as an absolute exceptional circumstance, I would like to dedicate this work to the members of my family who had to struggle at the end of their lives with the consequences of diabetic complications. Some of them, shortly before the finalization of this manuscript. This project enabled me to comprehend the full picture of their condition and silent clinical deterioration of type-2 diabetic patients.